CORE-SHELL COAXIALLY ELECTROSPUN COMPOSITE PCL/CHITOSAN WOUND HEALING BIOMATERIALS

A THESIS SUBMITTED TO
THE GRADUATE SCHOOL OF NATURAL AND APPLIED SCIENCES
OF
ATILIM UNIVERSITY

BY

SEDA SURUCU

THE DEPARTMENT OF METALLURGICAL AND MATERIALS ENGINEERING
JANUARY 2016

Approval of the Graduate School of Natural and Applied Sciences, Atılım University.

_____

Prof. Dr. Ibrahim K. Akman

I certify that this thesis satisfies all the requirements as a thesis for the degree of Master of Science.

_____

Prof. Dr. Naci SEVINC
Head of Department

This is to certify that we have read the thesis "Thesis Name" submitted by "Candidates Name" and that in our opinion it is fully adequate, in scope and quality, as a thesis for the degree of Master of Science.

_____

Assoc. Prof. Dr. Hilal TURKOGLU SASMAZEL
Supervisor

Examining Committee Members

Prof. Dr. Tulin Kutsal _____

Assoc. Prof. Dr. Jongee Park _____

Assoc. Prof. Dr. Hilal Turkoglu Sasmazel _____

Date: 26.01.2016

I declare and guarantee that all data, knowledge and information in this document has been obtained, processed and presented in accordance with academic rules and ethical conduct. Based on these rules and conduct, I have fully cited and referenced all material and results that are not original to this work.

Name, Last name: Seda, SURUCU

Signature:

ABSTRACT

CORE-SHELL COAXIALLY ELECTROSPUN COMPOSITE PCL/CHITOSAN WOUND HEALING BIOMATERIALS

Surucu, Seda

M.S., Metallurgical and Materials Engineering Department

Supervisor: Assoc. Prof. Dr. Hilal Turkoglu Sasmazel

January 2016, 57 pages

This study was related to combining of synthetic Poly (ε-caprolactone) (PCL) and natural chitosan polymers to form 3D PCL/chitosan core-shell structures for tissue engineering applications. The scaffolds were produced with electrospinning technique. The characterizations of the samples were done by contact angle (CA) measurements, scanning electron microscopy (SEM), transmission electron microscopy (TEM), X-Ray Photoelectron spectroscopy (XPS) analysis and also gas permeability test, mechanical test, thickness measurements, PBS absorption and shrinkage tests were performed for the scaffolds. The average inter-fiber diameter values were calculated as 0.717±0.001 μm for PCL, 0.660±0.007 μm for chitosan and 0.412±0.003 μm for PCL/chitosan core-shell structures, also the average inter-fiber pore size values exhibited decrease of 66.91% and 61.90% for the PCL and chitosan structures respectively, compared to PCL/chitosan core-shell structures. XPS analysis of the PCL/chitosan core-shell structures exhibited the characteristic peaks of PCL and chitosan polymers. The cell culture study was carried out with L929 ATCC CCL-1 mouse fibroblast cell line. Biocompatibility performance of the scaffolds was determined with MTT assay, fluorescence, Confocal Laser Scanning Microscope (CLSM) and SEM analysis. The results showed that the created micro/nano fibrous structure of the PCL/chitosan core-shell scaffolds in this study increased the cell viability and proliferation on/within scaffolds.

Keywords: PCL, chitosan, coaxiall electrospinning, tissue engineering, cell culture, fibroblasts.

ÖZ

EŞEKSENLİ ELEKTROEĞRİLMİŞ ÇEKİRDEK-KABUK TİPİ KOMPOZİT PCL/KİTOSAN YARA İYİLEŞME MALZEMELERİ

Sürücü, Seda
Yüksek Lisans, Metalurji ve Malzeme Mühendisliği Bölümü
Tez Yöneticisi: Doç. Dr. Hilal Türkoğlu Şaşmazel
Ocak 2016, 57 sayfa

Bu çalışma, sentetik poly(ε-caprolactone) (PCL) ve doğal kitosan polimerlerinin doku mühendisliği uygulamaları için 3 boyutlu PCL/kitosan/PCL çekirdek-kabuk yapıları oluşturmak üzere bir araya getirilmesi ile ilgilidir. Doku iskeleleri elektroeğirme yöntemi ile üretilmiştir. Numunelerin karakterizasyon özellikleri temas açısı ölçümü (CA), Taramalı Elektron Mikroskopu (SEM), Transmisyon Elektron Mikroskopu (TEM), X-ışını Fotoelektron Spektrometresi (XPS) analizleri ile belirlenmiş ve ayrıca doku iskeleleri için gaz geçirgenlik testi, kalınlık ölçümleri, PBS emme ve büzüşme testleri yapılmıştır. Ortalama fiberler arası çap değerleri PCL için 0.717±0.198 μm, kitosan için 0.660±0.070 μm ve PCL/kitosan çekirdek-kabuk yapısı için 0.412±0.339 μm olarak hesaplanmıştır. Ayrıca ortalama gözenek boyutları PCL/kitosan çekirdek-kabuk yapısına kıyasla sırasıyla PCL için %66.91 ve kitosan için %61.90 kadar düşüş göstermiştir. PCL/kitosan çekirdek-kabuk yapısının XPS analizi PCL ve kitosan polimerlerinin karakteristik tepe değerlerini göstermiştir. Hücre kültürü çalışması L929 ATCC CCL-1 fare deri hücre hattı ile yürütülmüştür. Doku iskelelerinin biyouyumluluk performansı MTT tahlili, floresan mikrosbu, Lazer Taramalı Konfokal Mikroskobu (CLSM) analizleri ile saptanmıştır. Sonuçlar göstermiştir ki bu araştırmadaki üretilen mikro/nano lifli PCL/kitosan çekirdek-kabuk doku iskelelerinin üzerinde ve içine doğru hücre canlılığı ve yayılması artmıştır.

Anahtar Kelimeler: PCL, kitosan, eşeksenli elektroeğirme, doku mühendisliği, hücre kültürü, deri hücresi.

To My Parents

ACKNOWLEDGMENTS

I would like to first and foremost show my sincere to my supervisor Assoc. Prof. Dr. Hilal Turkoglu Sasmazel. I learned lots of things from her. Without her immeasurable support, patience and guidance I could not prepare such a study. Each seconds of that study, she helped me with full patience and knowledge.

I would like to thank assistance Ozan Ozkan for his advice and supports. I am so thankful to him due to the time and the efforts that he spent to improve my skills.

I would like to thank to Metallurgical and Materials Engineering Department of Atilim University.

I would like to thank my family for their supports, patience and helps during my study.

Finally, I would like to thank to my boyfriend for his patience and encouragements.

TABLE OF CONTENTS

LIST OF TABLES

LIST OF FIGURES

LIST OF ABBREVIATIONS

PCL	-	Poly (ε-caprolactone)
ECM	-	Extracellular Matrices
TCPS	-	Tissue Culture Polystyrene
AF-488	-	Alexa Fluor 488 Phalloidin
XPS	-	X-Ray Photoelectron Spectroscopy
SEM	-	Scanning Electron Microscopy
TEM	-	Transmission Electron Microscopy
DD	-	Deacetylation Degree
TFA	-	Trifluoroacetic Acid
DC	-	Direct Current
CLSM	-	Confocal Laser Scanning Microscopy
PBS	-	Phosphate Buffer Saline
BSA	-	Bovine Serum Albumin
DMEM/F12	-	Dulbecco's Modified Eagle Medium
FBS	-	Fetal Bovine Serum

CHAPTER 1

Introduction

In the physiological medium and synthetic polymers with the advantage of no risk of infectious diseases and immune system reaction, natural polymers, biodegradability and solubility are widely used in tissue engineering applications [1-2]. Chitosan, whose name is a natural polymer, has very good features such as biodegradable, biocompatible, non-toxic and anti-thrombogenic [3-4]. However, PCL, a synthetic polymer, is biodegradable, extracted from the chemical synthesis of crude oil, having a low melting point of around 60°C and a glass transition temperature of about -60 °C with good mechanical properties [5-6]. The disadvantages of polymer types limit their individual usages as tissue scaffolds effectively. Therefore, the idea of usage of natural and synthetic polymers together as a single 3D hybrid scaffold is common. It has the advantages of both and the disadvantages of none which has been studied [7]. Three dimensional (3D) tissue scaffolds play a significant role in the subject named as tissue engineering. It serves as pre-formed extracellular matrices (ECM) on which cells attach to, grow and form new tissues [8-9]. Many bio-additive manufacturing techniques are able to produce 3D scaffolds with designed geometry and internal architectures [10-14]. One of the most preferred methods is the electrospinning process which ensures easy production of nanoscale continuous fiber structure of synthetic and natural polymers for the usage in tissue engineering application process.

Electrospun fibrous membranes which have high surface area in order to volume ratio have found applications in wound healing, tissue engineering, and drug delivery [15]. Electrospinning is a basic but very versatile method to produce micron and nanofibers from a variety of materials that include polymers, composites, and ceramics. The jet of polymer solution which is derived from the spinneret towards the counter electrode is continuously stretched because of the electrostatic repulsions between the surface charges. Also, there is a rapid evaporation of the solvent. Consequently, ultrafine fibers are stored on the counter electrode [16]. Coaxial

electrospinning was first introduced a decade ago. It has gained wide popularity ever since. It is applicable in different fields such as drug delivery, biotechnology and nanofluidics. A core–shell jet contains not only various polymer solutions but also a polymer solution as shell and a non-polymeric Newtonian liquid. It has even powder as core which is called electrospun coaxial electrospinning. At the exit of the core–shell needle a core–shell droplet appears, and degenerates a Taylor cone with the help of the high electric field acting on the liquid [17]. The liquid in the cone is subjected to sufficient strong electric field which emanates the form of a jet. It undergoes the electrical driven bending instability which is the characteristic of the electrospinning process. This process is accompanied by thinning of the jet and fast evaporation of the solvent. Ultimately, it results in the deposition of core–shell fibers on the counter-electrode. Coaxially electrospun fibers for tissue engineering application have been developed and then they are proved to be better than its individual and blended counterparts. Therefore, they are adopted in this work to develop potential fibrous samples as scaffolds for skin regeneration [18].

Our strategy in this study was to produce electrospun 3D PCL/chitosan core-shell structure for the tissue engineering usage as a scaffold. The main idea here was to fabricate composite tissue scaffolds by using coaxiall electrospinning technique in which PCL was used for the core layer and chitosan was used for shell layer. Optimum solution parameters such as chitosan and PCL solution concentration as well as electrospinning process parameters such as feed rate, applied voltage and spinneret-collector distance in order to obtain coaxiall fibers were determined with naked-eye observations, SEM and TEM analysis. Additionally, X-Ray Photoelectron spectroscopy (XPS) analyses, gas permeability test, mechanical test, thickness measurements, PBS absorption and shrinkage tests were performed characterize those produced PCL/chitosan core-shell structure. Finally, cell-material interactions of the candidate materials were investigated in vitro with L929 cell line over the course of 7 days.

CHAPTER 2

Literature Survey

2.1. Tissue Engineering

Tissue and organ failure occur as a result of injury or other type of damage. This is a major health problem, because it can estimate the half of the total annual expenditure in health care in the US [19]. Treatment options contain transplantation (human or xenotransplantation), surgical repairment, artificial prostheses, mechanical devices, and drug therapy but the major damage for a tissue or an organ cannot be repaired in a process of long-term recovery which is affected in a truly satisfactory way by these methods.

Tissue engineering comes out as a significant potential alternative or complementary solution. In other words, tissue and organ failure is addressed by implanting natural, synthetic, or semisynthetic tissue and organ mimics. These are actually functional from the start of the growth. Initial efforts have focused on skin equivalents for treating burns. However, there are an increasing number of tissue types which are now being engineered, as well as biomaterials and scaffolds that are used as delivery systems. A variety of approaches are used to coax differentiated or undifferentiated cells, such as stem cells and there are very notable results which include tissue-engineered bone, blood vessels, liver, muscle, and even nerve conduits. As a result of these, the medical and market potential become an important academic and corporate interest in this technology.

In the early development of tissue engineering, one of the significant components was the parallel development of artificial biomaterials. In the mid-1960s, artificial skin for burn victims was being followed as a symptomatic therapy [20]. After that, synthetic fibers were being used as artificial skin items for burn treatment [21]. In the early 1970s, there were many efforts to treat artificial surfaces to be used in implants in many ways. They would enable them to avoid causing blood coagulation as they use special heparin complex coatings [22]. Also, there are other efforts which focused on the toxicology profiles and biocompatibility of a variety of organic

polymers that are considered for implants or tissue engineering [23] in the process of the development of novel gels as the basis for artificial skin [24]. In the late 1970s, researchers experimented with collagen-based artificial skin which they used for oral mucosa injuries [25].

In this decade, several products reached the market. Interpore's Pro-Osteon coral-derived bone graft material was introduced in 1993. In 1996, Integra's Artificial Skin was approved as an in vivo, nonbiological tissue regeneration product. Then, in 1998, the General and Plastic Surgery Devices Advisory Panel to the US Food and Drug Administration (FDA) published unconditional approval of Apligraf (Graftskin) Human Skin Equivalent for the treatment of venous leg ulcers. Apligraf is the first manufactured living human organ produced by Organogenesis. It is a multilayered skin which was recommended for approval by an advisory panel to the FDA. Apligraf was approved for the treatment of venous leg ulcers in Canada in 1997. Later, it was launched in August 1997 by Novartis Pharmaceuticals Canada (Dorval, Canada).

Wound repair is an important application for tissue engineering products. Although most applications focus on the use of artificial skin to treat burns, there are also various disease conditions in which the use of artificial skin is beneficial. For example, Advanced Tissue Sciences' Dermagraft is a three-dimensional human neonatal dermal fibroblast culture. Also, it has been grown on a biodegradable scaffold and cryopreserved. Besides, it has been applied to foot ulcers developing as a side effect on long-term diabetes. Furthermore, in clinical trials, there are important healing applications occurred with this material. Especially, when the Dermagraft cells were alive and functioning properly [26].

2.1.1. Tissue Scaffolds

Tissue scaffolds play an important role in tissue engineering. A tissue scaffold is a three-dimensional (3D) structure which is made from biological materials and bio-materials. Indeed, it is used to facilitate tissue growth and the transport of nutrients in the process of upgrading itself. In order to produce tissue scaffolds, a number of fabrication techniques have been developed which can usually be separated into two categories: conventional and advanced. Conventional techniques

[27] which contain solvent-casting, particulate-leaching, and freeze drying, can produce scaffolds with interconnected porous structures although they offer little capacity so as to control pore size, pore geometry, pore interconnectivity, and spatial distribution of pores. At the same time, they enable the construction of internal channels within the scaffolds. Indeed, scaffolds should not only supply a supporting structure but also provide the chemical, mechanical, and biological signals to respond to environmental stimuli. In tissue engineering, advanced fabrication techniques have recently been developed such as electrospinning [28], a nanotechnology-based fabrication technique, and rapid prototyping [29] as an alternative to conventional scaffold fabrication methods. There is also a process of techniques. For example, a 3D scaffold is fabricated by laying down multiple formed layers. Consequently, with the development of such advanced tissue engineering fabrication techniques, the new concept of "biofabrication" has emerged. Biofabrication is known as the production of complicated living and non-living biological products which are derived from raw materials, such as living cells, molecules, extracellular matrices, and biomaterials. Actually, it has the potential to be the manufacturing paradigm of the 21st century. It also makes an important contribution to the development of tissue engineering strategies [30].

2.1.2. Natural and Synthetic Polymeric Tissue Scaffolds

In biomaterial research, scaffold design and fabrication are major areas. They are also crucial subjects for tissue engineering and regenerative medicine research [31]. Scaffold has a significant role in tissue regeneration and repair. Many works have been done thanks to applicable scaffold materials in tissue engineering in the past two decades. Scaffolds are named as three-dimension porous solid biomaterials. They are produced to perform some or all of the following functions: (i) supply cell-biomaterial interactions, cell adhesion, and ECM deposition, (ii) allow necessary transport of gases, nutrients, and regulating factors to provide cell survival, proliferation, and differentiation, (iii) biodegrade at a controllable rate which regulates the rate of tissue regeneration in the aspect of the culture conditions of interest, and (iv) promote a minimal degree of inflammation or toxicity in vivo [31]. The developing scaffolds are more reproducibly controlled in polymeric scaffolds through the optimal characteristics such as their strength, rate of degradation,

porosity as well as their shapes and sizes. There are few scaffolds that have displayed biological activity. They are used in the regeneration of tissues and organs that cannot regenerate them. Biological scaffolds are extracted from human or animal tissues and synthetic scaffolds which are derived from polymers. The first reports of induced regeneration of tissue are derived from an adult (dermis) by a scaffold in animals and humans. These tissues include peripheral nerve regeneration across a gap of unprecedented length and regeneration of the conjunctiva [33].

Polymers have been widely used tissue-engineering scaffolds in bioengineering field [34-35]. Due to their unique properties such as high surface-to-volume ratio, high porosity with very small size, biodegradation, and mechanical property, polymeric scaffolds have great care. They supply extraordinary advantages of biocompatibility, as well as versatility of chemistry, and the biological properties. These functions of polymeric scaffolds are very important in the application of tissue engineering and organ substitution. Researchers have achieved to grow skin and cartilage, bone and cartilage, liver [36], heart valves and arteries, bladder, pancreas, nerves, corneas, and various other soft tissues [37]. Actually, the main types of polymers are synthetic biodegradable and nonbiodegradable polymers which are also used as scaffold materials.

Natural polymers can be categorized as proteins (silk, collagen, gelatin, fibrinogen, elastin, keratin, actin, and myosin), polysaccharides (cellulose, amylose, dextran, chitin, and glycosaminoglycans), or polynucleotides (DNA, RNA). Owing to the bioactive properties, which provide better interactions with the cells, natural materials allow them to enhance the cells' performance in biological system. Natural polymers can be considered as the first biodegradable biomaterials which are used clinically [38].

Synthetic polymers gained high attraction for technical as well as medical application for various reasons. A wide range of physical and chemical properties can be achieved based on the monomer units, polymerization reaction and formation of co-polymers consisting of different components at adjustable concentrations. Technologies for synthesis and formation of complex shaped devices are mostly established. These types of polymers mainly fulfill structural and mechanical properties. Synthetic polymers, such as poly(glycolic acid) (PGA), poly(lactic acid) (PLA), poly(lactic-co-glycolic acid) (PLGA) and poly(ε-caprolactone) (PCL), have

been investigated as biomedical scaffold materials. Of them, PCL is biocompatible and biodegradable aliphatic polyester and has appropriate mechanical strength and good processability in many shapes, so it has been considered as a potential biomaterial for bone tissue regeneration [39].

2.1.2.1. Poly (ε-caprolactone) (PCL)

PCL has received considerable attention because of its biodegradability, favorable miscibility with other polymers and low temperature adhesiveness. PCL is aliphatic polyester made from ring opening polymerization of ε-caprolactone, a semi crystalline polymer with a melting point of 67˚C, glass transition temperature (Tg) in the range of -65 to -60˚C, and high elongation. When in composite, PCL can be used with plasticizers, such as poly(ethylene glycol) and glycerol [40]. PCL is a semi-crystalline polymer with the density of 1.145 g/cm^3 and has low melting temperature with crystallinity degree ranging from 45 and 67%. It is also widely used in production of scaffold in tissue engineering field [41]. Variation on its molar mass and crystallinity degree significantly affect its physical, mechanical, and thermal properties as well as its degradation rate, and PCL biodegradability can be improved by its combination with other polymers. The largest use of PCL is in the production of drug carriers, since this polymer is able to form structures (blended or not with other polymers) with high drug permeation. Furthermore, its degradation *in vivo* does not result in acidification of the microenvironment [42]. PCL has strong control over the scaffold′s pore shape, size, distribution and interconnectivity, which can mimic the natural extra cellular matrix of the organ/tissue to be replaced/regenerated. Hydrophobicity and lack of functional groups are major shortcomings of PCL scaffolds, which result in limited cell attachment and proliferation [43].

2.1.2.2. Chitosan

Chitosan, a partially deacetylated derivative of chitin, is a fibre-like substance consisting of glucosamine and N-acetylglucosamine and is soluble in dilute acids. It is structurally similar to glycosaminoglycans (GAG) which are important structural elements of the extracellular matrix (ECM) of many tissues. The density of chitosan is 0.15-0.3 g/cm^3. Chitosan has free amine groups and therefore possesses positive ionic charges, which facilitate its chemical binding with negatively charged lipids,

cholesterol, metal ions, proteins and macromolecules such as glycosaminoglycans and proteoglycans. This ability of chitosan for modification and combination with other polymers has allowed its use for the development of a wide range of scaffolds for the regeneration of many tissues such as the bone, liver, neural and vascular tissues, cartilage and skin [44].

The application of chitosan and its derivatives as biomaterials for wound healing has been widely reported. Various forms of chitosan have been tested in wound healing. In a comparative study of chitin, chitosan and water-soluble chitin (WSC) powders and WSC solution, WSC solution was found to have the highest tensile strength with the healing rate fastest for WSC solution, followed by WSC powder, chitin powder, and finally, chitosan powder. It is likely that the superior biodegradability and hydrophilicity of WSC can enhance its compatibility with wounded tissues and increase its activity as a wound-healing accelerator [45]. To improve the healing process, chitosan has been combined with a variety of modified materials such as growth factors, extracellular matrix components and antibacterial agents. It was found that the incorporation of basic fibroblast growth factor (bFGF) with chitosan accelerated the rate of healing [46].

2.2. Electrospinning Process

Electrospinning is a highly versatile spinning process. It is used for fiber formation which utilizes high electric field which is applied to the droplet of a solution or melt purging out from the tip of a capillary. It requires a DC voltage source in the range of several tens of kVs so as to produce electrostatic forces. The process is mainly based on the principle that strong electrical repulsive forces. It is produced by this voltage source that overcomes the weaker forces of surface tension in the liquid droplet. The electrostatic force is a phenomenon that is observed due to the electrostatic repulsions between similar charges in the liquid. It affects the liquid that causes the shape of the droplet to change from rounded meniscus to the Taylor cone. At this critical point, the applied electric field eventually becomes more prominent. It also overcomes the surface tension of the liquid leading to a jet of the solution ejected from the tip of the Taylor cone. Since the jet travels through the air, the flow changes from ohmic to convective because the charges go towards the surface of the fiber. In other words, it is an unstable whipping of the jet which emerges in the space between

the tip and the collector, which leads to evaporation of the solvent. By leaving the solid fiber behind, it causes a continuous fiber formation with diameters ranging from tens of nanometers to several micrometers [47-49]. The process should be carried out under properly ventilated chamber [50] because the possibilities of unpleasant or even harmful emissions of some polymers or solvent vapors occur during the spinning.

2.2.1. Parameters Affecting the Process

There are different parameters that have an effect on the electrospinning process. These parameters can be typically separated into two main categories; the first one is about solution parameters such as viscosity, conductivity, surface tension. The second one is about process parameters such as applied electric field, capillary-collector distance and feeding rate. Each of these groups is about parameters that can lead to different fiber morphologies and diameters. As a result, one can manage the desired fiber formation by proper manipulation of these parameters.

2.2.1.1. Solution Parameters

The spinnability of a polymer solution is based on the concentration. If polymer is too dilute, beads are shaped instead of fibers because of the effects of surface tension. If it is too intense, fibers cannot be formed as a result of the high viscosity but within the optimal range, fiber length and diameter should be proportional to the concentration [51].

Molecular Weight

Molecular weight of a polymer is a reflection of chain interactions such as Van der Waals attractions and entanglements. Thus, rheological and electrical properties of electrospinning solution deal with the molecular weight such as viscosity, surface tension, conductivity and dielectric strength [52]. Actually, the viscosity of a high molecular weight polymer in a solution will be higher compared to the viscosity of the same polymer with a lower molecular weight when it is compared [53].

Conductivity

Conductivity is an electrospinning solution which depends on various factors such as polymer and solvent type or charged ions in the solution. Since highly conductive solutions have greater charge and carrying capacities as opposed to low conductive

solutions which resulted in in sufficient elongation leading to bead formation, they are subjected to greater tensile forces under an electric field. Also, there are greater tensile forces which cause a decrease in fiber diameter. It is associated with the cube root of the solution conductivity as Baumgarten showed [54]. As most of the polymers are conductive, with a few exceptions of dielectric materials, the studies were carried out with different solvents, solution concentrations with the addition of ionic salts while controlling the effect of conductivity.

2.2.1.2. Process Parameters

Applied Electric Field

The applied voltage is an important element in the electrospinning process because an electric field is strong enough to overcome the surface tension of the liquid. In other words, it is required for fiber formation. There is a dispute among the researchers about the effect of applied voltage over fiber diameter. It is said that the diameter of electrospun fibers was not affected by the applied voltage [55] but there are some authors who have reported that larger fiber diameter is formed because of the increase in mass flow rate that is caused by the electrostatic force. On the other hand, other authors claimed that higher levels of voltage reduced the fiber diameter which is caused by stretching of the solution due to the greater columbic forces in the jet [56]. Also, the dispute is related to the correlation between voltage and bead formation. There are studies which are based on bead formation due to the high voltage as well as low voltage. Whereas one scenario showed that bead formation can occur at low voltages due to the slower feed rate, another scenario suggested that bead formation can occur at high voltages because of ejecting larger mass of solution.

Capillary-Collector Distance

The distance of capillary and the collector is another factor. It has effects on not only fiber diameter but also bead formation. A minimum distance is essential for solvent to evaporate if beaded morphology may be asked to be formed, but due to the longer stretching time [57], the longer period of solvent evaporation also decrease the fiber diameter. However, the effect of distance varies with the polymer which is used for the effect of distance varies Pham et al. [58] showed that for polysulfone, smaller distances have yielded smaller fibers.

Feeding Rate

The feeding of the electrospinning solution should be maintained at a certain level in order to keep Taylor cone present throughout the entire process. However, low feeding rate is desirable to provide enough time for solvent to evaporate for finer fiber diameter [58]. The most important effect of feed rate in electrospinning process is the formation of porous morphology on the fibers. Studies showed that pore size increases with the feed rate, more likely related to the amount of the solvent present during the jet formation [59].

2.2.1.3. Types of Electrospinning

Nowadays, the most basic electrospinning setup can be horizontal (Fig. 2.1). Besides, it can be vertical (Fig. 2.2) in terms of the layout with a single spinneret ejecting a single type of liquid but there are more sophisticated setups have been developed that can produce more complex nanofibrous structures in a more controlled and efficient manner with the increasing interest in this technology amongst several research groups. In order to get multilayered fiber mesh or a dual spinneret system that ejects two different solvents simultaneously to an alternating collector to stir the fibers into a single layer mesh, one of them is the sequential spinning of two different solvents. Dual spinneret system can be united for direct integration of cells into the fiber mesh by using a perpendicular capillary configuration while ejecting fiber and cells simultaneously onto a rotating mandrel moving on a linear stage [61]. Also, it is probable to produce composite and/or hybrid fibers which are basically **core-shell type** single fibers. It is obtained by *coaxial spinning* of two different polymer solutions from a single modified capillary tip [62]. These schematic representations of electrospinning setups can be seen in Fig 2.3 and 2.4. To summarize, the structural and topological properties of electrospun scaffolds can be changed with different experimental setups. They can be utilized as the number and/or design of the spinnerets or the design of the grounded collector plate. These can be stationary, rotating and/or alternating.

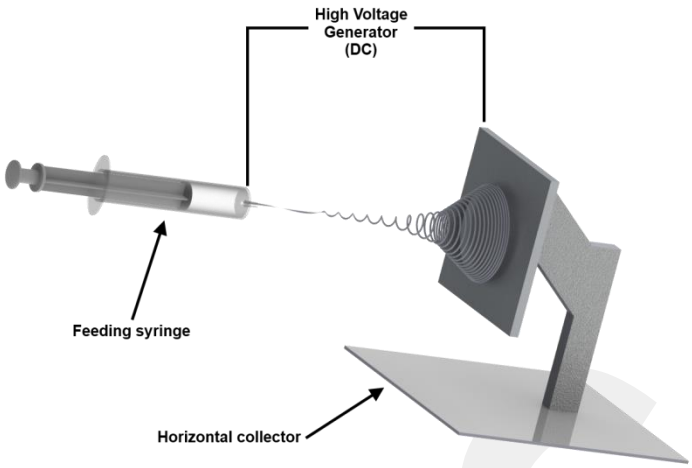

Figure 2.1. Schematic illustration of horizontal electrospinning setup.

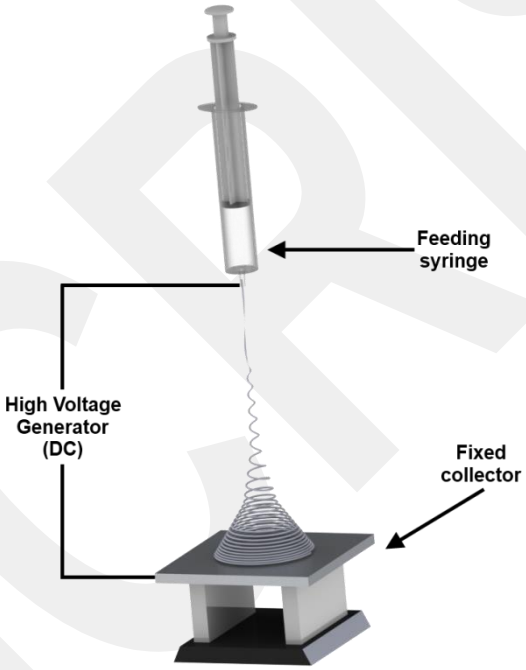

Figure 2.2. Schematic illustration of vertical electrospinning setup.

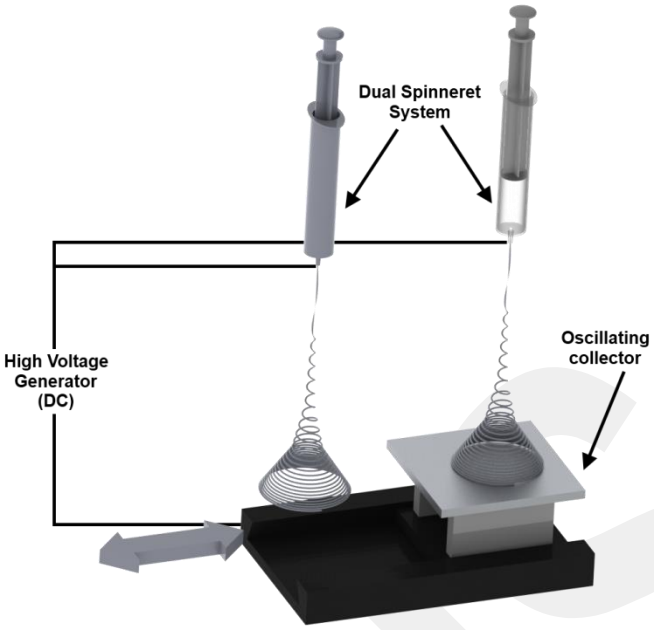

Figure 2.3. Vertical electrospinning setup with two seperate syringes and a horizontal osciallating collector for either sequential spinning to create multilayered mesh or dual spinning to create a single layer of mixed fibers.

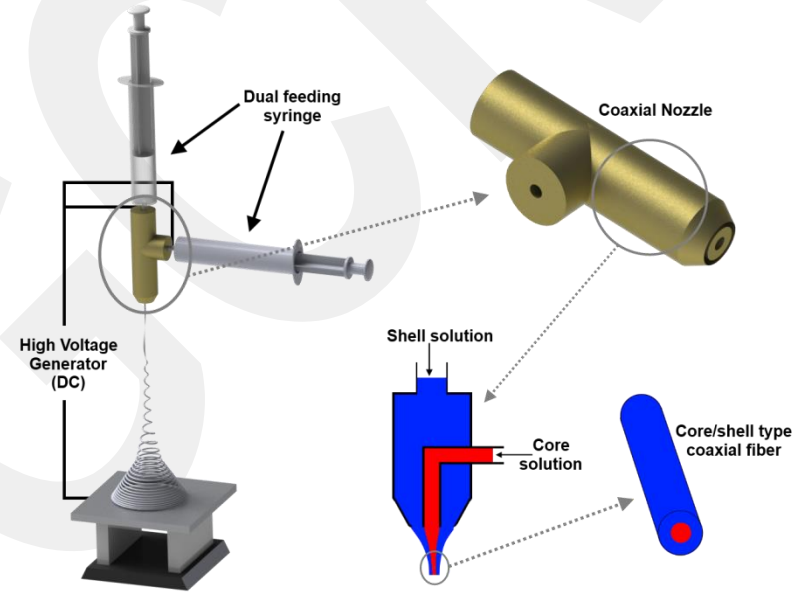

Figure 2.4. Coaxial electrospinning with modified nozzle configuration. One syringe to feed the core solution and the other to feed the shell solution into single two-component fibers.

2.2.1.4. Applications

Due to the several advantages, electrospinning process has a high surface area to volume ratio and a high porosity and some mechanical properties. Indeed, electrospinning process has gained increasing attention over the past decade. The desired morphological and mechanical properties for a specific application can be obtained because there are the manipulations of the solution and process parameters which can easily be done. There are also various studies of electrospinning for different applications. These have advantages of different properties of the process and the resulting structure. For example, while the fibrous structures supply mechanical support and anchorage location for the cells, it also has the ability to use and integrate various materials. Besides, therapeutic agents lead to a better restoration, maintenance, or improvement in **tissue engineering applications** whereas high surface area, that is used for the volume ratio and high and adjustable porosity, can provide better results in **filtration applications**. Since there is a requirement for selective permeability where the wound is needed to be protected from external pathogens while a certain humidity and nutrition conditions must be met for healing, the porosity can also be rewarding in wound dressing. **Drug delivery** is another field that benefits from the versatility of the electrospinning. It is also possible to create a controllable delivery system with different mechanisms such as diffusion, degradation or swelling thanks to the use of wide range of materials and therapeutic agents but, although there are different applications that require different properties, there is also one common reason that every application area can benefit from the process called "ease of use''.

Wound Dressing

Apart from tissue engineering scaffolds, wound dressing mats are protective covers which are used to promote healing and/or to prevent further harming of a wound. Due to this purpose, a definite porous structure is required to maintain a level of humidity and sustenance at the wound site. It is also impervious against exogenous pathogens. The effect of humidity, as firstly described by Winter [63], can be seen as the key point for a successful healing as a dry environment will cause dehydration of the collagen matrix in which the cells die and create a scab. Indeed, these prevent keratinocytes from penetrating the viable tissue. The required porous structure can be achieved in a fibrous as well as tissue engineering scaffolds. For example, Gu et al.

investigated electrospinning of gelatin and gelatin/poly(L-lactide) blend mats for wound dressing [64]. The resulting mats showed a water vapor permeation rate of 2569 g/m^2 /day which is very similar to the recommended value (2500 g/m^2 /day) proposed by Mi et al. [65]. By integrating substances that is known to be toxic to pathogens such as silver (Ag) Ag NPs are widely used for antibacterial effect in wound dressings. However, there are also other types of antibiotics. They can be added to the solution preparation phase in order to obtain a certain level of antibacterial protection in the electrospun mats. For example, Toncheva et al. investigated the antibacterial activity of electrospun mats based on poly(L-lactideco-D,L-lactide) (coPLA) and coPLA/poly(ethylene glycol) (PEG) containing a fluoroquinolone antibiotic: ciprofloxacin hydrochloride (Cipro), levofloxacin hemihydrate (Levo) or moxifloxacin hydrochloride (Moxi) against Staphylococcus aureus. All in all, the presence of the fluoroquinolone antibiotic both inhibited the bacterial growth and caused a substantial decrease/prevention in the adhesion of the pathogenic microorganisms [66].

CHAPTER 3
Experimental Study

3.1. Materials

Poly (ε-caprolactone) (PCL) (linear, MW=80,000 g/mol), chitosan (low molecular weight, 75-85% DD), trifluoroacetic acid (TFA), chloroform and methanol, which were used for the scaffold preparation, were purchased from Sigma-Aldrich (Germany). PBS (phosphate buffer saline) and BSA (bovine serum albumin) were obtained from Amresco (USA). Dulbecco's Modified Eagle Medium (DMEM/F12), penicillin/streptomycin, fetal bovine serum (FBS), ethanol (96%, v/v), glutaraldehyde, Triton X-100, acridine orange base, L-glutamine and propidium iodide were purchased from Sigma-Aldrich (USA). Also, Alexa Fluor 488 phalloidin was purchased from Life Technologies (USA). These chemicals were used at the cell culture studies.

3.2. Optimizations

3.2.1. Optimization of Solutions

In order to prepare electrospun PCL/chitosan core-shell scaffolds PCL and chitosan solution parameters and electrospinning process parameters were optimized. Optimization conditions were given in the following below tables (Table 3.1, 3.2, 3.3, 3.4, 3.5, 3.6, 3.7, 3.8 and 3.9)

Table 3.1. Preparation of PCL1 Solution.

Poly (ε-caprolactone)-1 PCL1*	
Poly (ε-caprolactone)	0.6 gr
Chloroform	3 ml
Methanol	1 ml
Temperature	30-35°C
Rotating Speed	200 rpm (20 min.)

*PCL1 solution with concentration of 15% (w/v) was prepared in chloroform and methanol (75/25 (v/v)) solvent.

Table 3.2. Preparation of PCL2 Solution.

Poly (ε-caprolactone)-2 PCL2*	
Poly (ε-caprolactone)	0.7 gr
Formic Acid	3 ml
Temperature	17-24˚C
Rotating Speed	200 rpm (20 min.)

* PCL2 solution with concentratation of 3% (w/v) was prepared in formic acid (glacial)/acetic acid (glacial) solvent.

Table 3.3. Preparation of Chitosan-1 Solution.

Chitosan-1 (CH1)*	
Chitosan	0.32 gr
TFA	4 ml
Temperature	55˚C
Rotating Speed	200 rpm (20 min.), 400 rpm (10 min.)

*Chitosan-1 solution with concentration of 8% (w/v) was prepared in TFA solvent.

Table 3.4. Preparation of Chitosan-2 Solution.

Chitosan-2 (CH2)*	
Chitosan	0.1 gr
Acetic Acid	0.2 ml
Temperature	30°C
Rotating Speed	200 rpm (20 min.), 400 rpm (5 min.)

*Chitosan-2 solution with concentration of 2% (w/v) was prepared in acetic acid solvent.

Table 3.5. Preparation of Chitosan-3 Solution.

Chitosan-3 (CH3)*	
Chitosan	0.2 gr
Acetic Acid	0.2 ml
Temperature	30°C
Rotating Speed	200 rpm (20 min.), 400 rpm (5 min.)

*Chitosan-3 solution with concentration of 3% (w/v) was prepared in acetic acid solvent.

Table 3.6. Preparation of Chitosan-4 Solution.

Chitosan-4 (CH4)*	
Chitosan	0.20 gr
TFA	5 ml
Temperature	55°C
Rotating Speed	200 rpm (20 min.), 400 rpm (10 min.)

* Chitosan-4 solution with concentration of 4% (w/v) was prepared in TFA solvent.

Table 3.7. Preparation of Chitosan-5 Solution.

Chitosan-5 (CH5)*	
Chitosan	0.1 gr
TFA	5 ml
Temperature	55°C
Rotating Speed	200 rpm (20 min.), 400 rpm (10 min.)

*Chitosan-5 solution with concentration of 2% (w/v) was prepared in TFA solvent.

Table 3.8. Preparation of Chitosan-6 Solution.

Chitosan-6 (CH6) *	
Chitosan	0.24 gr
TFA	4 ml
Temperature	55°C
Rotating Speed	200 rpm (20 min.), 400 rpm (10 min.)

* Chitosan-6 solution with concentration of 6% (w/v) was prepared in TFA solvent.

3.2.2. Optimization of Core-Shell Electrospinning Process

Table 3.9. Core-Shell Electrospinning Parameters.

#	Solution	Feeding (Chitosan)	Feeding (PCL)	Needle-Collector Distance	Voltage	Observation
1	PCL1-CH1	15 µl	2 µl	15 cm	15 kV	Not-Spinned
2	PCL1-CH1	15 µl	2 µl	15 cm	20 kV	Not-Spinned
3	PCL1-CH1	15 µl	5 µl	15 cm	15 kV	Not-Spinned
4	PCL1-CH1	15 µl	7 µl	15 cm	20 kV	Not-Spinned
5	PCL1-CH1	16 µl	7 µl	15 cm	20 kV	Not-Spinned

6	PCL1-CH1	16 µl	10 µl	15 cm	20 kV	Not-Spinned
7	PCL1-CH1	10 µl	10 µl	15 cm	20 kV	Not-Spinned
8	PCL1-CH1	6 µl	14 µl	15 cm	20 kV	Not-Spinned
9	**PCL1-CH1**	**2 µl**	**15 µl**	**15 cm**	**25 kV**	**Spinned**
10	PCL1-CH2	5 µl	2 µl	15 cm	15 kV	Not-Spinned
11	PCL1-CH2	10 µl	2 µl	15 cm	20 kV	Not-Spinned
12	PCL1-CH2	15 µl	5 µl	15 cm	15 kV	Not-Spinned
13	PCL1-CH2	15 µl	5 µl	15 cm	20 kV	Not-Spinned
14	PCL1-CH2	15 µl	5 µl	15 cm	25 kV	Not-Spinned
15	PCL1-CH2	15 µl	6 µl	15 cm	20 kV	Not-Spinned
16	PCL1-CH2	15 µl	6 µl	15 cm	25 kV	Not-Spinned
17	PCL1-CH2	16 µl	7 µl	15 cm	15 kV	Not-Spinned
18	PCL1-CH3	15 µl	7 µl	15 cm	20 kV	Not-Spinned

19	PCL1-CH3	5 µl	2 µl	15 cm	15 kV	Not-Spinned
20	PCL1-CH3	10 µl	2 µl	15 cm	20 kV	Not-Spinned
21	PCL1-CH3	15 µl	5 µl	15 cm	15 kV	Not-Spinned
22	PCL1-CH3	15 µl	5 µl	15 cm	20 kV	Not-Spinned
23	PCL1-CH3	15 µl	5 µl	15 cm	25 kV	Not-Spinned
24	PCL1-CH5	1 µl	1 µl	15 cm	30 kV	Not-Spinned
25	PCL1-CH5	1 µl	2 µl	15 cm	30 kV	Not-Spinned
26	PCL1-CH5	5 µl	10 µl	15 cm	30 kV	Not-Spinned
27	PCL1-CH5	3 µl	5 µl	15 cm	30 kV	Not-Spinned
28	PCL1-CH5	10 µl	5 µl	15 cm	30 kV	Not-Spinned
29	PCL1-CH4	10 µl	10 µl	15 cm	30 kV	Not-Spinned
30	PCL1-CH5	15 µl	2 µl	15 cm	30 kV	Not-Spinned
31	PCL1-CH5	15 µl	5 µl	15 cm	30 kV	Not-Spinned

32	PCL1-CH5	15 µl	10 µl	15 cm	25 kV	Not-Spinned
33	PCL1-CH5	15 µl	15 µl	15 cm	20 kV	Not-Spinned
34	PCL1-CH5	16 µl	2 µl	15 cm	30 kV	Not-Spinned
35	PCL1-CH5	16 µl	5 µl	15 cm	25 kV	Not-Spinned
36	PCL1-CH5	16 µl	10 µl	15 cm	30 kV	Needle-Spinned
37	PCL1-CH5	16 µl	15 µl	15 cm	25 kV	Needle-Spinned
38	PCL1-CH5	16 µl	20 µl	15 cm	25 kV	Needle-Spinned
39	PCL1-CH5	20 µl	5 µl	15 cm	25 kV	Needle-Spinned
40	PCL1-CH5	20 µl	15 µl	15 cm	25 kV	Needle-Spinned
41	PCL1-CH5	20 µl	20 µl	15 cm	25 kV	Needle-Spinned
42	PCL1-CH5	20 µl	25 µl	15 cm	25 kV	Needle-Spinned
43	PCL1-CH5	1 µl	1 µl	15 cm	30 kV	Not-Spinned
44	PCL1-CH5	1 µl	2 µl	15 cm	30 kV	Not-Spinned

45	PCL1-CH5	5 µl	10 µl	15 cm	30 kV	Not-Spinned
46	PCL1-CH5	3 µl	5 µl	15 cm	30 kV	Not-Spinned
47	PCL1-CH5	10 µl	5 µl	15 cm	30 kV	Not-Spinned
48	PCL1-CH4	10 µl	10 µl	15 cm	30 kV	Not-Spinned
49	PCL1-CH5	15 µl	2 µl	15 cm	30 kV	Not-Spinned
50	PCL1-CH5	15 µl	5 µl	15 cm	30 kV	Not-Spinned
51	PCL1-CH5	15 µl	10 µl	15 cm	25 kV	Not-Spinned
52	PCL1-CH5	15 µl	15 µl	15 cm	20 kV	Not-Spinned
53	PCL1-CH5	16 µl	2 µl	15 cm	30 kV	Not-Spinned
54	PCL1-CH5	16 µl	5 µl	15 cm	25 kV	Not-Spinned
55	PCL1-CH5	16 µl	10 µl	15 cm	30 kV	Needle-Spinned
56	PCL1-CH5	16 µl	15 µl	15 cm	25 kV	Needle-Spinned
57	PCL1-CH5	16 µl	20 µl	15 cm	25 kV	Needle-Spinned

58	PCL1-CH5	20 µl	5 µl	15 cm	25 kV	Needle-Spinned
59	PCL1-CH5	20 µl	15 µl	15 cm	25 kV	Needle-Spinned
60	PCL1-CH5	20 µl	20 µl	15 cm	25 kV	Needle-Spinned
61	PCL1-CH5	20 µl	25 µl	15 cm	25 kV	Needle-Spinned
62	PCL1-CH6	15 µl	2 µl	15 cm	15 Kv	Not-Spinned
63	PCL1-CH6	15 µl	2 µl	15 cm	20 kV	Not-Spinned
64	PCL1-CH6	15 µl	5 µl	15 cm	15 kV	Not-Spinned
65	PCL1-CH6	15 µl	7 µl	15 cm	20 kV	Not-Spinned
66	PCL1-CH6	16 µl	10 µl	15 cm	25 kV	Not-Spinned
67	PCL1-CH6	16 µl	12 µl	15 cm	25 kV	Not-Spinned
68	PCL1-CH6	16 µl	14 µl	15 cm	25 kV	Not-Spinned
69	PCL1-CH6	16 µl	7 µl	15 cm	25 kV	Not-Spinned
70	PCL1-CH6	20 µl	7 µl	15 cm	25 kV	Not-Spinned

71	PCL1-CH6	20 µl	10 µl	15 cm	25 kV	Not-Spinned
72	PCL1-CH6	10 µl	20 µl	15 cm	25 kV	Not-Spinned
73	PCL1-CH6	20 µl	15 µl	15 cm	25 kV	Not-Spinned
74	PCL1-CH6	20 µl	25 µl	15 cm	20 kV	Not-Spinned
75	PCL1-CH6	20 µl	25 µl	15 cm	25 kV	Not-Spinned
76	PCL1-CH6	20 µl	25 µl	15 cm	15 kV	Not-Spinned

3.3. Preparation of the Scaffolds

In this study, PCL/chitosan core-shell scaffolds were prepared by using electrospinning technique. For the first PCL solution, 15 wt% PCL was dissolved in chloroform/methanol mixture (75/25 v/v) for 20 min at 200 rpm and 30°C. For the chitosan, 8 wt% chitosan was dissolved in TFA for 25 min at 200 rpm and 50°C. The electrospun PCL/chitosan core-shell was electrospun at 15 cm capillary-collector distance and the applied voltage was 25 kV (Fig. 3.1).

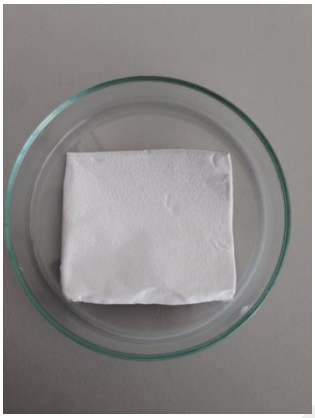

Figure 3.1. Macroscopic appearance of the electrospun PCL/chitosan core-shell scaffold.

3.4. Characterizations

3.4.1. Thickness

All electrospun scaffolds' thickness was measured through a micrometer; in other words, outside micrometer, 0-25 mm (USA) and for the sample batch, the average value was computed from 6 measurements of different scaffolds.

3.4.2. Contact Angle (CA) Measurements

The contact angle values of the electrospun PCL/chitosan core-shell scaffolds were measured as a function of surface tension of a series of liquids by using the sessile drop water contact angle measurement system (Phoenix 300, Surface Electro Optics, South Korea). Three samples were employed for each test, the average and the standard deviation values were calculated for each sample and compared to the reference surface wettability of commercial TCPS (Tissue Culture Polystyrene).

3.4.3. Scanning Electron Microscopy (SEM) Analysis

The electrospun PCL/chitosan core-shell samples were examined by using Image Scanning Electron Microscope (Quanta 400F FE-SEM, FEI, USA). The average fiber diameter and the average inter-fiber pore size values were calculated via ImageJ Launcher software program (USA) using SEM photographs.

3.4.4. Tranmission Electron Microscopy (TEM) Analysis

TEM observations (FEI Tecnai G2 Spirit BioTwin CTEM, (USA)) were carried out to determine the PCL/chitosan core-shell structure of the coaxially electrospun fibers. The samples for the TEM observation were prepared by putting the carbon-coated copper grid on the collector to directly deposit a very thin layer of electrospun fibers on the grid. Then, the copper grid containing fibers staining was used to take TEM image by passing a beam of electrons through.

3.4.5. Mechanical Properties

The electrospun PCL/chitosan core-shell scaffolds were cut into dog-bone shaped and the mechanical properties were obtained with a universal tensile testing instrument (Zwick/Roell 250 kN, Germany) with 100 N load cell.

3.4.6. Surface Chemistry Analysis

Chemical analysis of the near surface region for electrospun PCL/chitosan core-shell structure was done using X-ray photoelectron spectroscopy system (PHI 5000 Versa Probe, Physical Electronics, USA). Changing the material which was composed of surface functional carbon and oxygen groups was evaluated with high resolution scans.

3.4.7. PBS Absorption and Shrinkage Tests

The samples of the electrospun were cut into pieces in rectangular shapes by analyzing the dimensions of 10 mm x 5 mm for shrinkage and PBS absorption characteristics. After that, to measure their weights the samples were put in bottles, which contain 20 ml of PBS (pH = 7.4) and they were incubated in vitro at 37.0 ˚C for 24 h. The weights of the samples were measured and chosen by using an electronic balance. This process was occurred after removing the samples from PBS and blotting them with filter paper to absorb water on their surfaces. Through the following formula, the water uptakes of the electrospun samples in PBS were calculated.

$$A(\%) = \left(\frac{W_1 - W_0}{W_0} \right) x100$$

A is PBS absorption (%), W_0 (g) and W_1 (g) are the weights of the scaffolds and they appear before and after immersion in PBS medium for 24 h, respectively. In each group, three samples were recovered after they were being incubated in PBS and then dried in a vacuum oven for 12 h to remove the water for the PBS shrinkage test. The sizes of the dried samples were measured and the surface areas were calculated. To complete the evaluation, they were compared with the initial areas. As a result, the shrinkage percentage could be seen as the change ratio of the surface area change of the recovered scaffolds.

3.4.8. In Vitro Degradation

The in vitro degradation analyses of the electrospun PCL, chitosan and PCL/chitosan core-shell scaffolds was performed by using ASTM F 1635-04 method [67]. The electrospun PCL, chitosan and PCL/chitosan core-shell scaffolds were weighed and then immersed in 0.1 M PBS with pH 7.3, in three replicas containing 58.100 units/ml lysozyme. The storage of the samples was performed in test tubes, kept in an incubator at 37 ˚C. After periods of 1, 30, 60, 90, 120, 150 and 180 days of incubation, the samples were removed from the medium and washed with distilled water and dried in vacuum oven for 24 h to remove excess water and weighed the weight remaining was calculated.

$$Weight\ remaining(\%) = 100 - \left(\frac{W_0 - W_d}{W_0} \times 100 \right)$$

W_0 and W_d are the weights of the electrospun scaffolds before and after degradation for a specific time interval, respectively.

3.4.8.1. SEM Observations

After the 60 days of incubation, the samples (single electrospun PCL and electrospun PCL/chitosan core-shell scaffolds) were taken from incubator and the samples were examined by using Image Scanning Electron Microscope (Quanta 400F FE-SEM, FEI, USA).

3.4.9. Water Vapor Transmission Rate (WVTR)

Water vapor transmission rate was determined by using ASTM E69 method [68]. 10 ml of distilled water was put into the cup, then square shape of the PCL, chitosan and

PCL/chitosan core-shell scaffolds with dimensions of 50x50 mm and thicknesses of 2 mm were sealed tightly on the mouth of the cylindrical cup (50 mm diameter) with parafilm. Prepared specimens placed in the incubator at 37˚C. Water vapor transmission measurements were repeated every 3h for 24h period for each samples. The results are presented as a mean value with a standard deviation (n=6). Water vapor transmission rate (g/m^2.day) was calculated from the following equation:

$$WVTR = \frac{W_0 - W_f}{A \times 10^6} \text{ g/m}^2\text{.day}$$

Where, W_0 (gram) and W_f (gram) are the weights of the cup before and after being placed in an incubator, filled with the given amount of water and sealed with samples, A (mm^2) is the mouth area of the cup.

3.5. Cell Culture Studies

Cell culture studies were carried out by L929 ATCC CCL-1 mouse fibroblast cell line obtained from Kirikkale University Bioengineering Laboratory in order to observe cell-material interactions. Cells were seeded on the prepared scaffolds with the concentration of 1x10^5 cells/ml and the culture was incubated under 5% CO_2 at 37°C and monitored for 7 days, where DMEM/F12 + %10 (v/v) FBS + 1% (v/v) penicillin+streptomycin (100 units/ml penicillin, 100 μg/ml streptomycin) was used as culture medium. The samples were cut as circular, 1 cm diameter and placed in each parafilm coated TCPS (tissue culture Polystyrene) well. Additionally before culture, prepared samples were sterilized with UV for 30 min. Cell growth was determined with MTT assay and the seeded scaffolds were examined by fluorescence, confocal and scanning electron microscopes for adhesion, growth and proliferation characteristics.

3.5.1. MTT Assay

The electrospun PCL-only, chitosan-only and PCL/chitosan core-shell nanofiber samples were placed in parafilm coated 24 well-plates and MTT assay was carried out every 48 hours, starting with 24 hours after the seeding time for 7 days of the cell culture period. The medium solution was added to each well and allowed incubation for every 24 hours at incubation condition. After incubation, the cultured samples were removed from the incubator, the medium of the scaffolds was discarded and the

samples were washed with PBS for 3 times. After washing, 600 µl fresh medium and 60 µl MTT solution were added to each well and incubated for 3 hours. After the incubation, MTT solution of the samples was discarded and 1 ml dimethylsulfoxide (DMSO) added to each well and incubated for 1 hour. Then 200 µl solutions were taken from each well and placed into 96 well-plates. The absorbance values were measured with a microplate reader at 540 nm and the cell viability was observed comparatively for PCL-only, chitosan-only and PCL/chitosan core-shell nanofiber and TCPS Petri dishes as control groups and each measurement was done for 3 replicas.

The MTT cell proliferation assay measures the cell proliferation rate and conversely, when metabolic events lead to apoptosis or necrosis measures the reduction in cell viability. The viability of the cells in a culture is directly related to the level of reduction, which can easily be assessed with a spectrometer.

3.5.2. Fluorescence Imaging

In order to observe cell attachment and proliferation on/within the electrospun PCL/chitosan core-shell structures, scaffolds were stained with Acridine Orange (AO, 10 µg/ml). Fluorescent images were taken on the 3rd, 5th and 7th days. For the imaging, the cultured samples were taken from the incubator, the medium on the samples was discarded and each scaffold was washed 3 times with PBS. Then the samples were fixed with 4% (v/v) paraformaldehyde for 45 min. Following the fixation, the samples were stained with AO solution for 10 mins in the dark and the images were taken with Fluorescent Microscope (AMG EVOS-FL, USA) immediately thereafter.

3.5.3. Confocal Laser Scanning Microscope Analysis

The cultured samples were also observed with Confocal Laser Scanning Microscope on the 3rd and 7th days. The samples were removed from incubator and the medium was discarded. After washing 3 times with PBS, the samples were fixed with 4% v/v paraformaldehyde for 60 min and immersed in 0.1% Triton X-100 for 5 min in order to increase cell permeability. Then the samples were incubated in Alexa Fluor 488 Phalloidin (AF-488) and DRAQ5 staining solutions for 20 min and 10 min, respectively. After the incubation, the samples were washed with PBS. The images

were obtained with Confocal Laser Scanning Microscope (Zeiss LSM 510, USA) where the excitation and the emission wavelengths were λ_{ex}: 488 nm and λ_{em}: 500-550 nm for AF-488, and λ_{ex}: 635-640 nm and λ_{em}: 655-700 nm for DRAQ5.

3.5.4. Observation with SEM

The morphological characteristics of the cells cultured on the modified samples were observed by Scanning Electron Microscopy (SEM) at the end of the 3rd and 7th day of the culture. Therefore, the medium in each well was discarded after the samples were removed from the incubator, and each scaffold was washed 3 times with PBS. Following the fixation with 2.5% v/v glutaraldehyde for 30 min, the samples were dehydrated for 2 min sequentially with 30%, 40%, 50%, 60%, 70%, 80%, 90% and 100% ethanol solutions. Finally, the samples were immersed in 100% hexamethyldisilazane for 5 min, air-dried and coated with Au-Pt (~3 nm) before SEM imaging.

CHAPTER 4
Results and Discussion

4.1. Optimizations

Electrospinning was not observed with PCL2 solution, therefore it was eliminated. PCL1 and CH1 solutions with the given properties in the Table 3.1 and 3.3 were selected for the future studies according to our experiences and previous studies [70]. According to the Table 3.9, for experiments with the numbers of 1-8, 10-35, 43-54 and 62-76, it was observed that chitosan was collected on the tip of the needle, therefore chitosan solution could not have power to lift up the PCL solution. For experiments with the numbers of 36-42, 55-61, it was observed that the solutions were frozen after a while. After cleaning the tip of the needle, fibers continued to electrospin. Therefore, no continuous electrospinning of the fibers were observed for those experiments. Continuous electrospun fibers were obtained with the experiment of number 9. Therefore, core-shell electrospinning process parameters were determined according to the experiment number 9 (Table 3.9).

4.2. Characterizations

4.2.1. Thickness, The Average Fiber Diameter and The Average Inter-Fiber Pore Size Values of The Prepared Electrospun Scaffolds

By using a micrometer and ImageJ Launcher software program (USA) which was being used from SEM photographs, the thicknesses were measured and the average fiber diameter and the average inter-fiber pore size were summarized in Table 4.1. It is clearly understood from the measurements that the thicknesses of the prepared scaffolds were almost the same, in the range of 0.019 ± 0.006 - 0.021 ± 0.003 mm.
According to the results of average fiber diameter measurements, the highest and the lowest values of the average fiber diameters were derived from the PCL (0.717 ± 0.001 μm) and the PCL/chitosan core-shell structure (0.412 ± 0.003) scaffolds, respectively.

Table 4.1. Properties of the electrospun PCL/chitosan core-shell scaffolds.

Sample	Thickness (mm)	Average fiber diameter (μm)	Average inter-fiber pore size (μm)
PCL	0.019 ± 0.006	0.717 ± 0.001	1.076 ± 0.494
Chitosan	0.020 ± 0.001	0.660 ± 0.007	1.209 ± 0.404
PCL/chitosan core-shell	0.021 ± 0.003	0.412 ± 0.003	3.173 ± 0.650

4.2.2. Contact Angle Measurements

The contact angle values of the electrospun single PCL, single chitosan and PCL/chitosan core-shell scaffolds were shown in Table 4.2. As seen in the table, electrospun PCL is a hydrophobic material with a contact angle value over 100°. On the contrary, chitosan is highly hydrophilic due to its OH groups on the chain; hence, the PCL/chitosan core-shell scaffold had a moderate hydrophilicity (78.214˚ ± 2.544) due to the combination of single PCL with single chitosan materials. In the literature it is reported that comparing with hydrophobic structure, hydrophilic and/or moderately hydrophilic structures support cell attachment and then cell growth better.

Table 4.2. The contact angle (CA) values (˚) of the electrospun single PCL, single chitosan and PCL/chitosan core-shell scaffolds.

Sample	Contact angle (CA) (˚)
Single PCL layer	114.015 ± 3.154
Single chitosan layer	-*
Layer by layer PCL/chitosan/PCL	78.214 ± 2.544

** Contact angle value of chitosan could not be measured.*

4.2.3. Scanning Electron Microscope (SEM) Analysis

The morphology of the nanofibers was observed by scanning electron microscopy (SEM). The SEM micrographs and diameter distributions of electrospun PCL/chitosan core-shell scaffolds with different weight ratios were shown in Fig. 4.1 and it was easy to form continuous nanofibers, which might show a large number of homogeneous structures [69]. It could be seen that the uniform electrospun PCL/chitosan core-shell scaffolds had smooth and homogeneous morphology (Fig. 4.1).

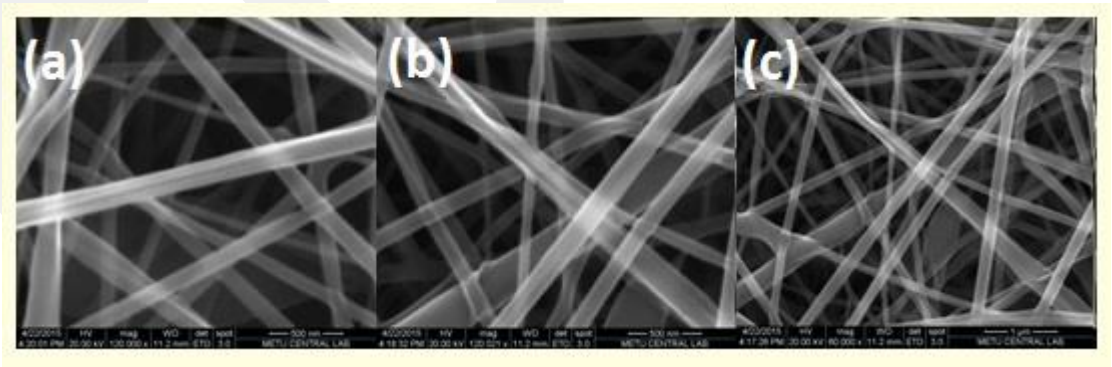

Figure 4.1. SEM images of electrospun PCL/chitosan core-shell scaffolds (a) x120000, (b)x120000, (c)x60000.

4.2.4. Transmission Electron Microscope (TEM) Analysis

Two immiscible liquids were fed through two concentrically arranged needles, with their sharp ends blunted to facilitate a formation of a stable jet. The inner diameters of the needles were 0.9 and 0.57 mm, respectively. The flow of solution through the inner needle was controlled by a syringe pump. Due to its history of being successfully electrospun into robust, porous non-woven samples and being able to support cell proliferation, PCL was used as a model polymer to form the core structure of the nanofibers. The chitosan solution containing TFA was selected as model shell contents.

The distance between the syringe exit and collector was 15 cm, the electrical voltage was 25 kV, the flow rate of the inner dope was at 15.0 μl/min, outer dope was 2.0 μl/min and the ambient temperature was around 24 ˚C.

Fig. 4.2 shows TEM pictures of the core/shell structures of the PCL/chitosan core-shell scaffolds fabricated at the core feed rates. The density of PCL (core) was higher than that of chitosan (shell). Hence fewer electrons were transmitted through the PCL core, leading darker observation. As shown in Fig. 4.2(d) and (e), the core layer of PCL was completely encapsulated by the outer layer of chitosan at the core feed rate of 15.0 μl/min. The interface between the core and shell layers was clearly observed. By using a spinneret composed of two coaxial capillaries, two components could be fed through inner and outer coaxial capillary channels and electrospun simultaneously [71].

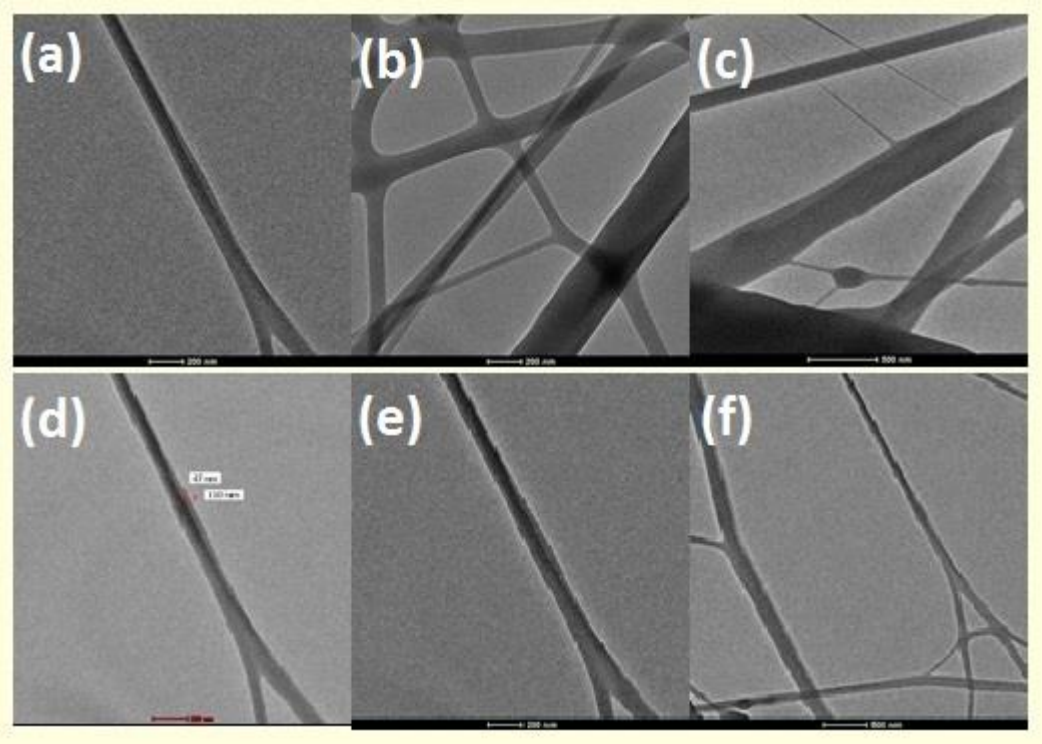

Figure 4.2. TEM images of the coaxially electrospun composite nanofibers of the PCL/chitosan core-shell scaffolds fabricated at shell feed rate of 2.0 μl/min and core feed rate of (a), (b), (c), (d), (e) and (f) 15 μl/min.

4.2.5. Mechanical Properties

Mechanical strength of nanofibrous scaffolds is very important for tissue engineering applications. Table 4.3 summarizes the mechanical properties of the prepared scaffold (Elastic Modulus, Tensile Strength). The average elastic modulus and tensile strength values were found as 1.330 ± 0.002, 0.668 ± 0.023 and 0.909 ± 0.040, 0.451 ± 0.010 for the PCL and chitosan scaffolds, respectively. The single chitosan nanofibers were found to have low elastic modulus as well as low tensile strength, compared to the single PCL nanofibers. On the other hand, the core-shell structured PCL-chitosan nanofibers were found to have increased elastic modulus (3.284 MPa ± 0.016) and tensile strength (1.318 MPa ± 0.042) and decreased the strain at break value (11.000% ± 2.345), compared to the single chitosan and single PCL nanofibers. Therefore, combining PCL and chitosan in a core-shell structure decreased the elastic and plastic deformation under the same amount of load applied. Additionally, the strain at break value was the lowest in PCL/chitosan core-shell scaffolds comparing to single PCL and single chitosan scaffolds; therefore,

PCL/chitosan core-shell scaffolds were more brittle, resulting less elongation before failure.

Table 4.3. Tensile properties of the electrospun PCL/chitosan core-shell scaffolds.

Sample	Elastic Modulus (MPa)	Tensile Strength (MPa)	Strain at break (%)
PCL	1.330 ± 0.002	0.909 ± 0.040	77.020 ± 3.000
Chitosan	0.668 ± 0.023	0.451 ± 0.010	40.090 ± 2.500
PCL/chitosan core-shell	3.284 ± 0.016	1.318 ± 0.042	11.000 ± 2.345

4.2.6. Surface Chemistry Analysis

The X-ray photoelectron spectrum (XPS) analysis was analyzed to gain insight for the chemical composition and binding states on the surface of the PCL/chitosan core–shell structure. The binding energies obtained as a result of the XPS analysis and they were corrected for specimen changing by referring C1s to 285 eV. In the survey spectrum in Fig. 4.3 the main elements on the surface of the nanostructure are C and O Fig. 4.4 and 4.5 presents the high-resolution XPS spectra of O1s, the peak located at around 531 eV is ascribed to the lattice oxygen. Through the analyses, it was seen that the characteristic components' peaks of the PCL and chitosan expected from PCL/chitosan core-shell scaffold, which were C-C (285 eV), C*-COO (285.6 eV), C-OH, C*-OCO (286.6 eV), COO, COOH (288.83 eV), C=O (532.1 eV) and C-O (531 eV) (Fig. 4.4, 4.5 and Table 4.4**)**. PCL/chitosan core-shell scaffold' C1s and O1s compositions were found 67.8% and 32.2%, respectively.

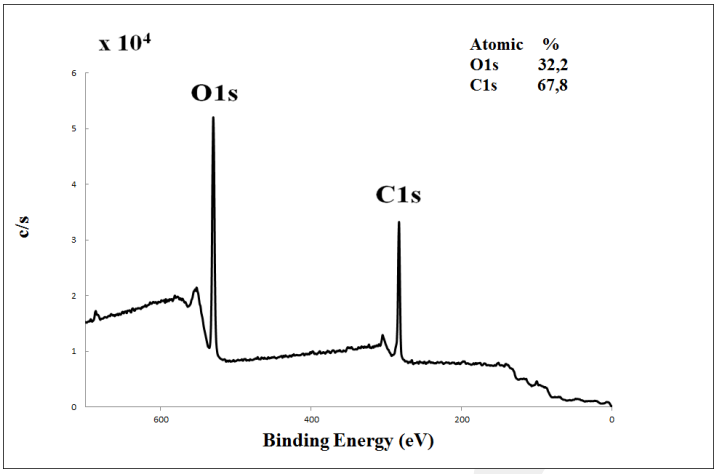

Figure 4.3. Survey scan of the electrospun PCL/chitosan core-shell scaffolds.

Table 4.4. Surface composition (atomic %) of the PCL/chitosan core-shell scaffolds.

eV	**Group**	**PCL/Chitosan core-shell**	
		Area	%
285.00	C-C	11308	38
285.60	C*-COO	6684	30
286.20	C-N		
286.60	C-OH, C*-OCO	5289	18
288.83	COO, COOH	4556	15
eV	**Group**	**Area**	**Ratio**
532.10	C=O	11456	1.20
531.00	C-O	9354	

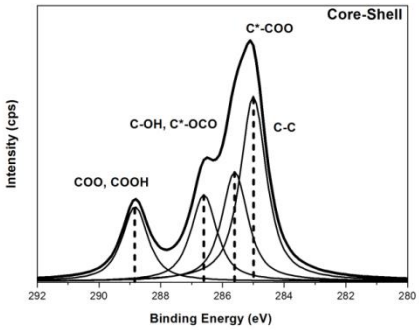

Figure 4.4. High resolution scans of C1s (285eV) spectrums for electrospun PCL/chitosan core-shell scaffolds.

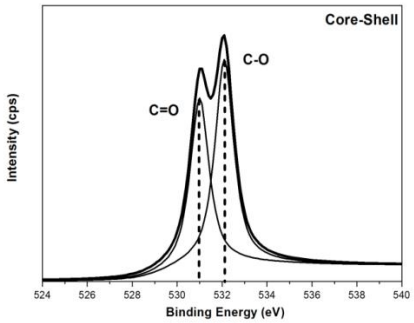

Figure 4.5. High resolution scans of O1s (531 eV) spectrums for electrospun PCL/chitosan core-shell scaffolds.

4.2.7. PBS Absorption and Shrinkage Tests

Table 4.5 shows the shrinkage and PBS absorption characteristics of the electrospun scaffolds. The electrospun single electrospun PCL scaffold showed PBS absorption value as 12.7%, which contributed to its hydrophobic nature. By mixing the hydrophobic component (PCL) with the hydrophilic component (chitosan), the nanofibrous composite scaffold of PCL/chitosan core-shell structure increased its PBS uptake to 88.08%. Through the PCL/chitosan core-shell structure scaffolds, it is seen that the PBS absorption values of 88.08% which were higher than the absorption values of the single electrospun PCL scaffolds.

Table 4.5. Shrinkage and PBS absorption characteristics of the electrospun scaffolds.

Sample	PBS Absorption (%)	Shrinkage (%)
PCL	12.7 ± 3.8	1.7 ± 1.5
PCL/Chitosan Core-Shell	88.08 ± 2.4	5.6 ± 1.4

4.2.8. In Vitro Degradation

The in vitro degradation of the single chitosan, single PCL and PCL/chitosan core shell scaffolds, shown as weight remaining after degradation, was depicted in Fig. 4.6. Overall, PCL/chitosan core-shell scaffolds showed milder degradation than the PCL after 7 days of incubation. Single PCL, with the highest value weight remaining (%), lost very little weight throughout the entire process compared with single chitosan and PCL/chitosan core-shell scaffolds. As the value weight remaining (%) increased, the degradation rate reduced. Single chitosan had the fastest degradation rate of 100% weight loss after 7 days of incubation, while PCL/chitosan core-shell slower degradation rate of only 7.2% weight loss. After 30 days of incubation, 7.3% and 27.5% weight loss values were observed for the single PCL and PCL/chitosan core-shell scaffolds, respectively. However, after 60 days of incubation, PCL/chitosan core-shell scaffold showed a higher weight loss value (50%) than single PCL scaffold (10%). This may also be larger pore size of PCL/chitosan core-shell scaffolds, which allows high network structures to be exposed to lysozyme, resulting in increased degradation rates.

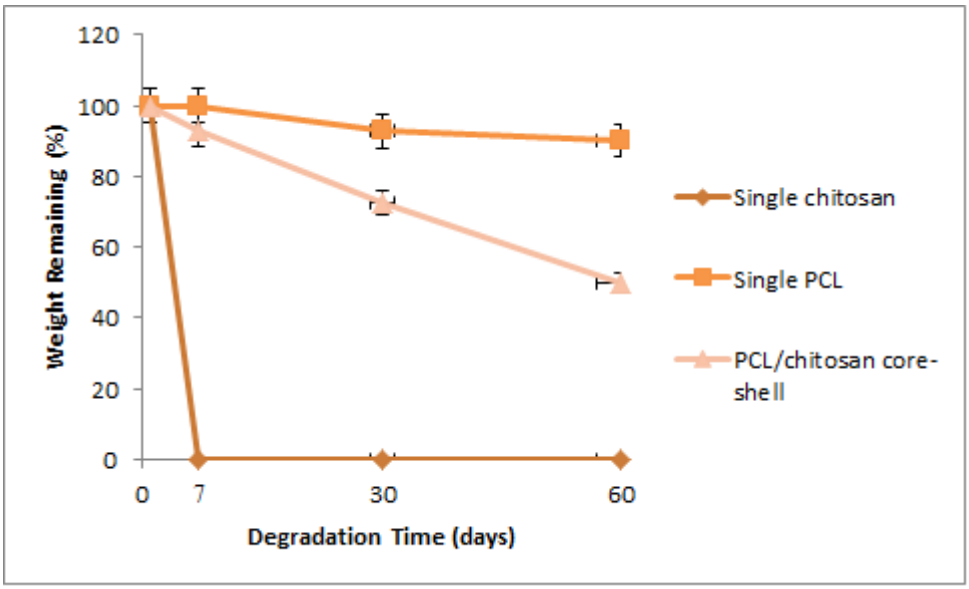

Figure 4.6. Weight remaining of different single chitosan, single PCL and PCL/chitosan core-shell scaffolds as a function of degradation time.

4.2.8.1. SEM Observations

Lysozyme is known to be ubiquitous in the body [72]. Since lysozyme is present in cellular lysosomes and lysosomal rupture is associated with inflammation, it has been assumed that the source of the increased lysozyme activity is the release of enzyme from the lysosomes of phagocytic cells [73]. The main advantage of biodegradable over non-biodegradable materials is the disappearance of implanted foreign material, which could elicit foreign body reactions from the host's defense system during their long-term contact with a living structure. It is expected that, when the scaffolds are implanted in the body, the PCL/chitosan core-shell scaffolds will be degraded gradually by lysozyme and then reabsorbed. In the presence of lysozyme, it was possible to detect the preferential attack of PCL/chitosan core-shell scaffolds since this enzyme is able to hydrolyze PCL/chitosan core-shell in some extent. The SEM photographs showing decent degradation obtained in this work proved the attack of PCL/chitosan core-shell scaffolds by lysozyme through the larger size of the pores of the scaffolds with the help of chitosan combination. The smooth SEM photographs belonging to single PCL scaffolds indicated slower/lower degradation of the scaffolds (Fig. 4.7).

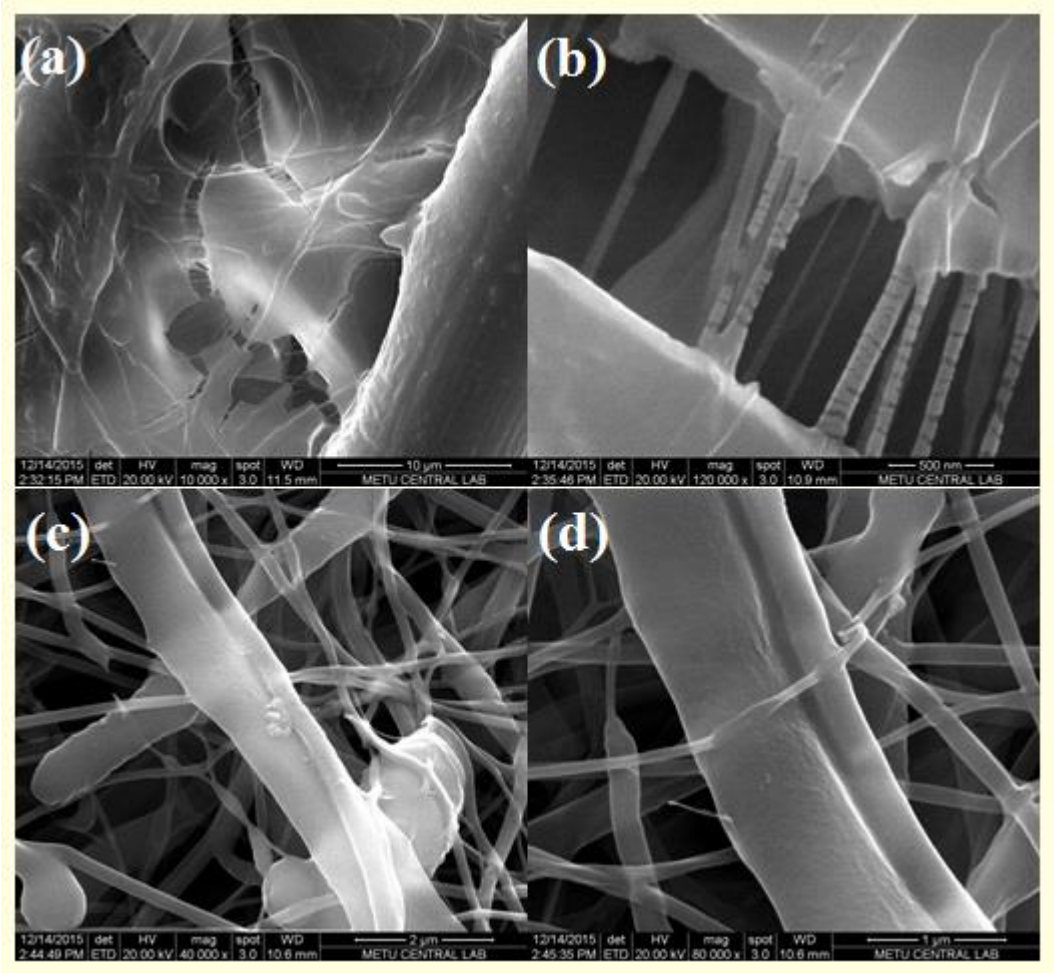

Figure 4.7. SEM images showing the morphology of electrospun PCL/chitosan core-shell scaffolds after 60 days with lysozyme (a) x10000; (b) x120000; PCL scaffolds (d) x40000; (e) x80000.

4.2.9. Water Vapor Transmission Rate (WVTR)

The most difficult problem in treating a burned skin was the fact that the victim may have lost most of its body liquid due to evaporation and exudation. These will affect the decrease of body temperature and accelerate the rate of metabolism. Therefore, the wound dressing must avoid or at least reduce the body liquid lost, i.e. by controlling absorption and transmission as well as by maintaining the high humidity in the wound area, in order to accelerate the formation of granule and epithelialization process. On the other hand, if the WVTR is low, then accumulation of exudates will occur, this may cause the deceleration of healing process and opens up the risk of bacterial growth. In the literature, it was reported the evaporative water loss for normal skin as 204 ± 12 g/m^2.day and that for injured skin can range from

279 ± 26 g/m^2.day for a first degree burn to 5138 ± 202 g/m^2.day for a granulating wound. The water vapor permeability of a wound dressing should prevent excessive dehydration as well as buildup of exudates. It has been recommended that a rate of 2000-2500 g/m^2.day would provide adequate level of moisture without risk in wound dehydration [74-75]. WVTR results for three types of scaffolds were shown in Table 4.6. The single electrospun PCL scaffold exhibited the lowest average WVTR value among the scaffolds. Since the single PCL scaffolds have the lowest average inter-fiber pore size compared with the other scaffolds, the results obtained for WVTR value for these scaffolds were meaningful. The average WVTR value of single electrospun chitosan scaffolds were higher than single electrospun PCL scaffolds' value but lower than PCL/chitosan core-shell scaffolds' value. The highest value of the WVTR belonged to PCL/chitosan core-shell scaffolds. The increase of the average inter-fiber pore size in PCL/chitosan core-shell scaffolds significantly supported these results obtained here. It was observed that the developed PCL/chitosan core-shell and chitosan scaffolds met the requirements of an ideal wound dressing in terms of water vapor transmission rate.

Table 4.6. Water vapor transmission rate of PCL, chitosan and PCL/chitosan core-shell scaffolds.

Samples	WVTR (g/m^2.day)
PCL	1654±3.2
Chitosan	2254±2.6
PCL/chitosan core-shell	2315±3.4

4.3. Cell Culture Studies

4.3.1. MTT Assay

MTT assay results for every 48 hours showed that all of the scaffolds caused no toxicity for fibroblast cells and a steady increase in cell viability for 7 days (Fig. 4.8). At the end of the 7th day of the cell culture, the highest cell growth and proliferation were obtained by PCL/chitosan core-shell nanofibers. Previous studies showed that synthetic polymers offered a suitable mechanical and biodegradable characteristic but lacked of native biocompatibility as that of natural polymers, yet essential to provide good interaction between the cells and biomimetic ECM [76]. Therefore, the combined form of those synthetic PCL and natural chitosan as core-shell electrospun structure made by micro and nano sized fibers with interfiber pores, which was biomimicking native ECM structure of PCL/chitosan core-shell, supplied the highest cell growth and proliferation on/within the PCL/chitosan core-shell scaffolds at the end of the culture. Additionally, 3D network of those produced PCL/chitosan scaffolds played an important role to give the cells a higher surface to volume ratio resulting in higher cell density. The results were consistent with the literature Merkle et. al. [77] obtained similar results with muscle cells on the gelatin scaffolds and coaxial scaffolds; gelatin had the lowest cell spreading, while 3Gel/1PVA coaxial scaffolds the highest amount of cell spreading. They found that all scaffolds possessed cellular viability greater than 80% with the gelatin and coaxial scaffolds possessing a higher viability than the only PVA scaffolds. Wang et. al. [78] successfully examined in vitro cell attachment and proliferation on the PVDF/PVP core-shell structure and it could be seen that statistically significant differences ($p < 0.05$) were observed in the cell activity of L929 cell line culturing for 24 h, 48 h and 72 h in the presence of PVDF/PVP nanofiber extract. They found that, compared to the control group, all the results indicated that PVDF/PVP nanofiber had a good biocompatibility, which made it as a good potential wound dressing for skin regeneration. Fig. 4.8 showed herein that the proliferation of L929 cells on the chitosan nanofibrous structures was relatively lower than that on the combining PCL and chitosan nanofibrous structure. This was attributed to the small pore size which packed densely by nanofibers, owing to the use of the traditional electrospinning process to prepare chitosan nanofibers and also due to super hydrophilic structure.

Although single electrospun PCL scaffold had 3D structure, its hydrophobic feature didn't allow us to get higher cell proliferation on/within that scaffold compared with TCPS well which had moderate wettability at the end of the culture.

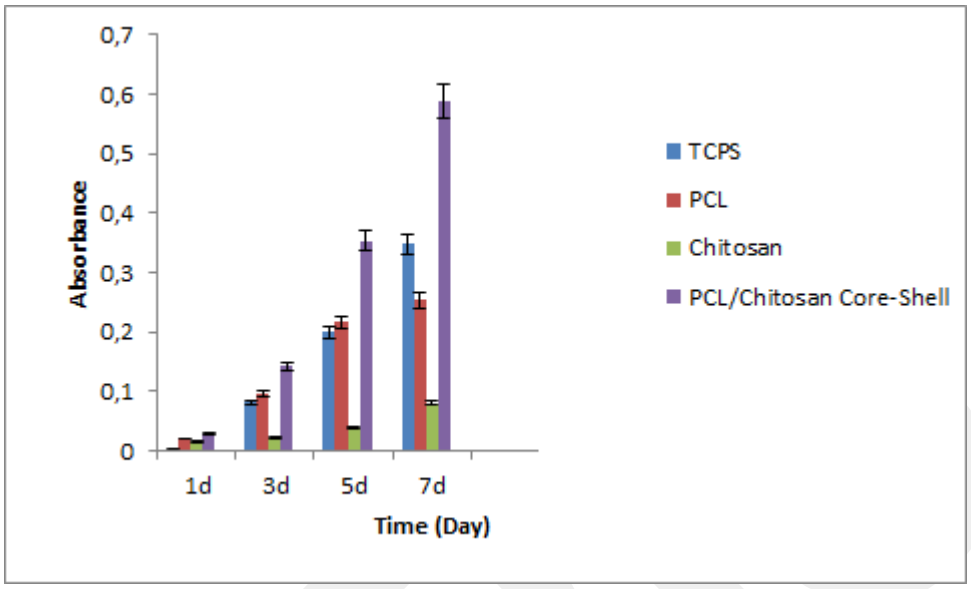

Figure 4.8. Absorbance values of control (TCPS Petri dishes), the electrospun PCL, chitosan and PCL/chitosan core-shell scaffolds.

4.3.2. Fluorescence Imaging

On the 3rd, 5th and 7th days of the culture, the PCL/chitosan core-shell scaffolds were examined under fluorescent microscope in order to observe fibroblast cell attachment and proliferation (Fig. 4.9). The images obtained on the 7th day showed that the density of L929 fibroblast cells increased excessively on the surface and inward while maintaining their characteristic phenotype as they proliferate. This increased cell yield on/within the electrospun PCL/chitosan core-shell scaffolds owing to the increase specific interface area at a nanoscale, formed by covering random PCL microfibrous matrix with random chitosan nanofibers. Such an architecture promoted cell attachment and microstructure obtained infiltration of cells within the scaffold. These results showed the statements that the combination of synthetic PCL and natural chitosan polymers to form composite fibrous membranes would lead to a suitable design of biomimetic ECM providing both appropriate mechanical characteristics and chemical composition.

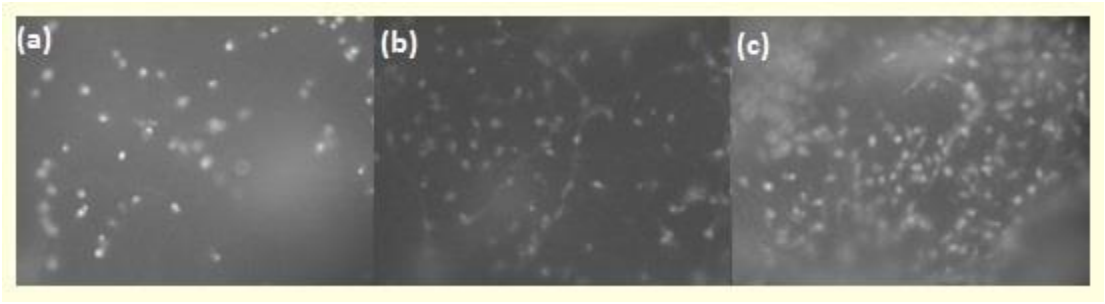

Figure 4.9. Fluorescent microscope images; PCL/chitosan core-shell scaffolds on (a) 3rd day, (b) 5th day (c) 7th day. The magnification of the images is x20.

4.3.3. Confocal Laser Scanning Microscope Analysis

Cell culture on/within PCL/chitosan core-shell scaffolds was observed by confocal laser scanning microscope on the 3rd and 7th days of the culture (Fig. 4.10). The cells showed the expected morphology with a fusiform or spindle-like shape depending on the cell response on/within the scaffolds.

On the 3rd day of the culture, the cells were able to attach to the matrix and proliferate and growth as clusters, possibly aided by electrostatic interactions with the matrix. On the 7th day of the culture the density of the cells increased in PCL/chitosan core-shell scaffolds and tended to align. The number of nuclei increased in the scaffolds. These results were similar to those obtained with the MTT assay in particular. The results confirmed the increased proliferation on/within the PCL/chitosan core-shell scaffolds.

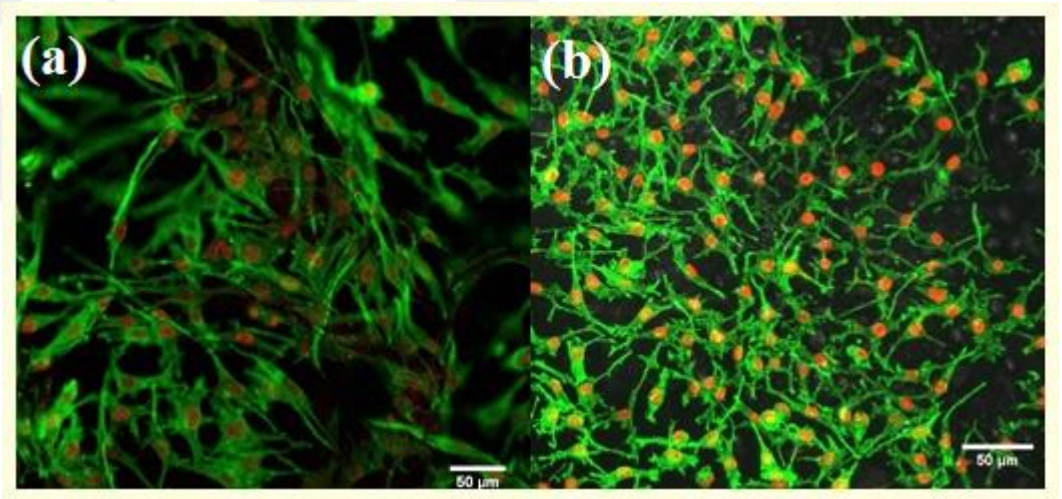

Figure 4.10. Confocal microscope images; PCL/chitosan core-shell scaffolds on (a) 3rd day, x20; (b) 7th day, x10.

4.3.4. Observation with SEM

The morphology of L929 mouse fibroblast cells cultured on/within the PCL/chitosan core-shell scaffolds of the 3rd and 7th cultured days was shown in Fig. 4.11. The cells spread on the surface of the PCL/chitosan core-shell scaffolds by their filopodia and they penetrated inside the pores. It was observed that the cells attached well on the matrix and were either round (on the 3rd day) or flat (on the 7th day) in morphology. SEM images suggested that the scaffolds were biocompatible and could be considered as suitable scaffolds for wound healing applications which were complementary of the MTT assay results of the study. Martins et al. [79] confirmed that the adhesion, spreading, and growth of both fibroblast and osteoblast cells are enhanced by blending chitosan with starch, which was in agreement with the result of this study.

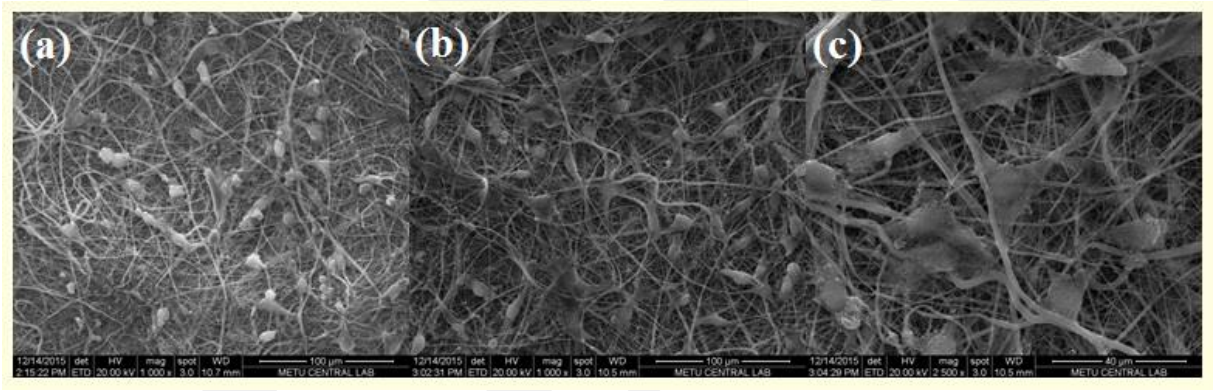

Figure 4.11. SEM images of the electrospun PCL/chitosan core-shell scaffolds on the (a) 3rd day of culture, x1000; (b) 7th day of culture, x1000 (c) 7th day of culture, x2500.

CHAPTER 5
Conclusions

- According to the measurements the thicknesses of the prepared scaffolds were almost the same, in the range of 0.019 ± 0.006 - 0.021 ± 0.003 mm and the average fiber diameter measurements, the highest and the lowest values of the average fiber diameters were derived from the PCL (0.717 ± 0.198 μm) and the PCL/chitosan core-shell structure (0.412 ± 0.339) scaffolds, respectively.
- The results of CA values showed that the PCL/chitosan core-shell scaffold had a moderate hydrophilicity (78.214° ± 2.544) due to the combining of PCL with chitosan materials.
- According to SEM and TEM analysis, the uniform electrospun PCL/chitosan core-shell scaffolds had smooth and homogeneous morphology and the density of PCL (core) was higher than that of chitosan (shell). Hence fewer electrons were transmitted through the PCL core, leading darker observation. The core layer of PCL was completely encapsulated by the outer layer of chitosan at the core feed rates of 15.0 μl/min. The interface between the core and shell layers was clearly observed.
- The average elastic modulus and tensile strength values were found as 1.330 ± 0.002, 0.668 ± 0.023 and 0.909 ± 0.040, 0.451 ± 0.010 for the PCL and chitosan scaffolds, respectively. The chitosan-only nanofibers were found to have low elastic modulus as well as low tensile strength, compared to the PCL-only nanofibers. On the other hand, the core-shell structured PCL-chitosan nanofibers were found to have increased elastic modulus tensile strength, compared to the chitosan-only and PCL-only nanofibers. Therefore, combining PCL and chitosan in a core-shell structure decreased the elastic and plastic deformation under the same amount of load applied.
- Through the XPS analyses, it was seen that the characteristic components' peaks of the PCL and chitosan expected from PCL/chitosan core-shell

scaffold, which were C-C (285 eV), C*-COO (285.6 eV), C-OH, C*-OCO (286.6 eV), COO, COOH (288.83 eV), C=O (532.1 eV) and C-O (531 eV). PCL/chitosan core-shell scaffold' C1s and O1s compositions were found 67.8% and 32.2%, respectively.

- The PCL/chitosan core-shell structure scaffolds, it was seen that the PBS absorption values which were higher than the absorption values of the electrospun PCL scaffolds for PBS absorption and shrinkage test.
- The SEM photographs showing decent degradation obtained in this work proved the attack of PCL/chitosan core-shell scaffolds by lysozyme through the larger size of the pores of the scaffolds with the help of chitosan combination and also belonging to single PCL scaffolds indicated slower/lower degradation of the scaffolds.
- The highest value of the WVTR belonged to PCL/chitosan core-shell scaffolds. The increase of the average inter-fiber pore size in PCL/chitosan core-shell scaffolds significantly supported these results obtained here.
- The effect of these developed materials on the cell attachment and growth were examined by MTT assay methods and fluorescence, CLSM and SEM imaging. The PCL/chitosan core-shell supplied the highest cell growth and proliferation on/within the PCL/chitosan core-shell scaffolds at the end of the culture. Additionally, 3D network of those produced PCL/chitosan scaffolds played an important role to give cells higher surface to volume ratio resulting in higher cell density.

CHAPTER 6

References

[1] Seman H, Wozney JM. Delivery of bone morphogenetic proteins for orthopedic tissue regeneration. Cytokine Growth Factor Rev 2005;16:329-45.

[2] Lee SH, Shin H. Matrices and scaffolds for delivery of bioactive molecules in bone and cartilage tissue engineering. Adv Drug Deliv Rev 2007;59:339-59.

[3] Kumirska J. et al. Application of spectroscopic methods for structural analysis of chitin and chitosan. Mar Drugs 2010;8:1567-636.

[4] Kumar MNVR. Review of chitin and chitosan applications. React Funct Polym 2000;46:1-27.

[5] Maher PS. et al. Construction of 3D bio- logical matrices using rapid prototyping technology. Rapid Prototyp J 2009;15:204-10.

[6] Maher PS. et al. Formed 3D bio-scaffolds via rapid prototyping technology. In: van der Sloten J, Verdonck P, Nyssen M, Haueisen J, editors. IFMBE Proceedings. USA: Springer; 2009. p. 2200-4.

[7] Chung J, Park TG. Surface engineered and drug releasing pre-fabricated scaffolds for tissue engineering. Adv Drug Deliv Rev 2007;59:149-262.

[8] Zeltinger J. et al. Effect of pore size and void fraction on cellular adhesion, proliferation, and matrix deposition. Tissue Eng 2001;7:557-72.

[9] Zein I. et al. Fused deposition modeling of novel scaffold architectures for tissue engineering applications. Biomaterials 2002;23:1169-85.

[10] Jain RA. The manufacturing techniques of various drug loaded biodegradable poly(lactide-co-glycolide) (PLGA) devices. Biomaterials 2000;21:2475-90.

[11] Hutmacher DW. et al. Mechanical properties and cell cultural response of polycaprolactone scaffolds designed and fabricated via fused deposition modeling. J Biomed Mater Res 2001;55:203-16.

[12] Yildirim ED. et al. Fabrication and plasma treatment of 3D polycaprolactone tissue scaffolds for enhanced cellular function. Virtual Phys Prototyping 2008;3:199-207.

[13] Shor L. et al. Precision extruding deposition (PED) fabrication of polycaprolactone (PCL) scaffolds for bone tissue engineering. Biofabrication 2009;1:13-21.

[14] Liu XH, Ma PX. Polymeric scaffolds for bone tissue engineering. Ann Biomed Eng 2004;32:477-86.

[15] Taepaiboon P, Rungsardthong U, Supaphol P. Drug-loaded electrospun mats of poly(vinyl alcohol) fibres and their release characteristics of four model drugs. Nanotechnology 2006;17:2317–22.

[16] Ga HL, Jun-Cheol S, Keun-Byoung Y. Controlled wall thickness and porosity of polymeric hollow nanofibers by coaxial electrospinning. Macromol Res 2010;18:571-6.

[17] Reznik SN. et al. Evolution of a compound droplet attached to a core shell nozzle under the action of a strong electric field. Phys Fluids 2006;18:1-13.

[18] Reneker DH, Yarin AL. Electrospinning jets and polymer nanofibers. Polymer 2008;49:2387-425.

[19] Langer R, Vacanti JP. Tissue Engineering. Science 1993;260:920-6.

[20] Hall CW, Liotta D, Debakey M. Artifical skin. ASAIO 2001;12:340-5.

[21] Spira et al. Evaluation of synthetic fabrics as artificial skin grafts to experimental burn wounds. J Biomater Res 2009;3:213-34.

[22] Mansbridge J. et al. Three-dimensional fibroblast culture implant for the treatment of diabetic foot ulcers: Metabolic activity and therapeutic range. Tissue Eng 1998;4:403-414.

[23] Sawyer AA. et al. The stimulation of healing within a rat calvarial defect by mPCL–TCP/collagen scaffolds loaded with rhBMP-2. Biomaterials 2009;30:2479-88.

[24] Misuzu Y. et al. Simvastatin inhibits osteoclast differentiation induced by bone morphogenetic protein-2 and RANKL through regulating MAPK, AKT and Src signaling. Regul Peptides 2010;162:99-108.

[25] Matthias WL, Michael DM. Prevascularization in tissue engineering: Current concepts and future directions. Biotechnol Adv 2015; doi:10.1016/j.biotechadv.2015.12.004.

[26] Lallepak L. et al. Silk sericin: A versatile material for tissue engineering and drug delivery. Biotechnol Adv 2015;33:1855-67.

[27] Liu C, Xia Z, Czernuszka JT. Design and development of three-dimensional scaffolds for tissue engineering. Chem Eng Res Des 2007;85:1051-64.

[28] Prabhakaran MP, Ghasemi-Mobarakeh L, Ramakrishna S. Electrospun composite nanofibers for tissue regeneration. J Nanosci Nanotechno 2011;11:3039-57.

[29] Peltola SM. et al. A review of rapid prototyp- ing techniques for tissue engineering purposes. Ann Med 2008;40:268-80.

[30] Mironov V. et al. Biofabrication: a 21st century manufacturing paradigm. Biofabrication 2009;1:022001.

[31] Langer R, Tirrell DA. Designing materials for biology and medicine. Nature 2004;428:487-92.

[32] Fuchs JR, Nasseri BA, Vacanti JP. Tissue engineering: a 21st century solution to surgical reconstruction. Ann of Thoracic Surg 2001;72:577-91.

[33] Piskin E. Biodegradable polymers as biomaterials. J Biomater Sci Polym Ed 1994;6:775-95.

[34] Ji Y, Ghosh K, Shu XZ. Electrospun three-dimensional hyaluronic acid nanofibrous scaffolds. Biomaterials 2006;27:3782-92.

[35] Mayer J. et al. Matrices for tissue engineering-scaffold structure for a bioartificial liver support system. J Control Release 2000;64:81-90.

[36] Mohammad J. et al. Modulation of peripheral nerve regeneration: a tissue-engineering approach. The role of amnion tube nerve conduit across a 1-centimeter nerve gap. Plast Reconstr Surg 2000;105:660-6.

[37] Nair LS, Laurencin CT. Biodegradable polymers as biomaterials. Prog Polym Sci 2007;32:762-98.

[38] Yannas IV. Classes of materials used in medicine: natural materials. In: Ratner BD, Hoffman AS, Schoen FJ, Lemons J, editors. Biomat Sci-An Introduction to Materials in Medicine, Elsevier Academic Press, San Diego, Calif, USA, 2004. p. 127-36.

[39] Duarte AR, Mano JF, Reis RL. Supercritical phase inversion of starch-poly(ε-caprolactone) for tissue engineering applications. J Mater Sci Mater Med 2010;21:533-40.

[40] Gorrasi G. et al. Correlations between microstructural characterization and thermal properties of well defined poly(ε-caprolactone) samples by ring opening

polymerization with neutral and cationic bis(2,4,6-triisopropylphenyl)tin(IV) compounds. React Funct Polym 2010;70:151-8.

[41] Labet M, Thielemans W. Synthesis of polycaprolactone: a review. Chem Soc Rev 2009;38:3484-504.

[42] Wei X. et al. Biodegradable poly(ε-caprolactone)–poly(ethylene glycol) copolymers as drug delivery system. Int J Pharm 2009;381:1-8.

[43] Sinha VR. et al. Poly-ε-caprolactone microspheres and nanospheres: an overview. Int J Pharm 2004;278:1-23.

[44] Shi C. et al. Therapeutic potential of chitosan and its derivatives in regenerative medicine. J Surg Res 2006;133;185-92.

[45] Cho YW. et al. Water-soluble chitin as a wound healing accelerator. Biomaterials 1999;20:2139.

[46] Obara K. et al. Photocrosslinkable chitosan hydrogel containing fibroblast growth factor-2 stimulates wound healing in healing-impaired db/db mice. Biomaterials 2003;24:3437.

[47] Taylor GI. Electrically driven jets. P Roy Soc Lond A Mat 1969; 313:453-75.

[48] Yarin AL, Koombhongse S, Reneker DH. Bending instability in electrospinning of nanofibers. J Appl Phys 2001;89:3018-26.

[49] Adomaviciute E, Rimvydas M. The influence of applied voltage on poly (vinyl alcohol) (PVA) nanofibre diameter. Fibers Text East Eur 2007; 15:64–5.

[50] Huang ZM. et al. A review on polymer nanofibers by electrospinning and their applications in nanocomposites. Compos Sci Technol 2003;63:2223-53.

[51] Thompson CJ. et al. Effects of parameters on nanofiber diameter determined from electrospinning model. Polymer 2007;48:6913-22.

[52] Shenoy SL. et al. Role of chain entanglements on fiber formation during electrospinning of polymer solutions: good solvent, non-specific polymer–polymer interaction limit. Polymer 2005;46:3372-84.

[53] Koski A, Yim K, Shivkumar S. Effect of molecular weight on fibrous PVA produced by electrospinning. Mater Lett 2004;58:493-7.

[54] Baumgarten PK. Electrostatic spinning of acrylic microfibers. J Colloid Interface Sci 1971;36:71-9.

[55] Tan SH. et al. Systematic parameter study for ultrafine fiber fabrication via electrospinning process. Polymer 2005;46:6128-34.

[56] Zhang C. et al. Study on morphology of electrospun poly (vinyl alcohol) mats. Eur Polym J 2005;41:423-32.

[57] Doshi J, Reneker DH. Electrospinning process and applications of electrospun fibers. J Electrostatics 1995;35:151-60.

[58] Yuan XY. et al. Morphology of ultrafine polysulfone fibers prepared by electrospinning. Polym Int 2004;53:1704-10.

[59] Touny AH, Bhaduri SB. A reactive electrospinning approach for nanoporous PLA/monetite nanocomposite fibers. Mater Sci Eng C 2010;30:1304-12.

[60] Sun Z. et al. Compound core–shell polymer nanofibers by co-electrospinning. Adv Mater 2003;22:1929-32.

[61] Matthews JA. et al. Electrospinning of collagen nanofibers. Biomacromolecules 2002; 3:232-8.

[62] Carnell LS. et al. Aligned mats from electrospun single fibers. Macromolecules 2008;41:5345-9.

[63] Winter GD. Formation of the scab and the rate of epithelization of superficial wounds in the skin of the young domestic pig. Nature 1962;193:293.

[64] Gu SY. et al. Electrospinning of gelatin and gelatin/poly(l-lactide) blend and its characteristics for wound dressing. Mater Sci Eng C 2009;29:1822-8.

[65] Mi FL. et al. Fabrication and characterization of a sponge-like asymmetric chitosan membrane as a wound dressing. Biomaterials 2001;22:165-73.

[66] Pant B. et al. Characterization and antibacterial properties of Ag NPs loaded nylon-6 nanocomposite prepared by one-step electrospinning process. Colloid Surface A 2012;395:94-9.

[67] Annual Book of ASTM Standards, ASTM F 1635-04: Standard Test Method for in vitro Degradation Testing of Hydrolytically Degradable Polymer Resins and Fabricated Forms for Surgical Implants, 1995;4:1-5.

[68] Annual Book of ASTM Standards, ASTM E96: Standard Test Methods for Water Vapor Transmission of Materials, 1995;04.06:785-92.

[69] Yajing L, Fan C, Jun D. Electrospun poly(lactic acid)/chitosan core–shell structure nanofibers from homogeneous solution, Carbohyd Polym 2012;90:1445-51.

[70] Turkoglu Sasmazel H. Novel hybrid scaffolds for the cultivation of osteoblast cells. Int J Biol Macromol 2011;49:838-46.

[71] Díaz JE. et al. Controlled encapsulation of hydrophobic liquids in hydrophilic polymer nanofibers by coelectrospinning. Adv Funct Mater 2006;16:2110-6.

[72] Hankiewicz J, Swierczek E. Lysozyme in human body fluids. Clin Chim Acta 1974;57:205-9.

[73] Brouwer J, Vanleeuwenherberts T, Ottingvanderuit M. Determination of lysozyme in serum, urine, cerebrospinal-fluid and feces by enzyme-immunoassay. Clin Chim Acta 1984;142:21-30.

[74] Ching TT. et al. Evaluation of chitosan/-poly(glutamic acid) polyelectrolyte complex for wound dressing materials. Carbohyd Polym 2011;84:812-9.

[75] Kim IY. et al. Evaluation of semi-interpenetrating polymer networks composed of chitosan and poloxamer for wound dressing application. Int J Pharm 2007;341:35-43.

[76] Sheng-Han C. et al. A three-dimensional dual-layer nano/micro fibrous structure of electrospun chitosan/poly(D,L-lactide) membrane for the improvement of cytocompatibility. J Membrane Sci 2014;450:224-34.

[77] Valerie MM. et al. Core–shell PVA/gelatin electrospun nanofibers promote human umbilical vein endothelial cell and smooth muscle cell proliferation and migration. Acta Biomater 2015;27:77-87.

[78] Wang M. et al. Preparation of PVDF/PVP core-shell nanofibers mats via homogeneous electrospinning. Polym 2014;55:2188-96.

[79] Martins AM. et al. Natural origin scaffolds with in situ pore forming capability for bone tissue engineering applications. Acta Biomater 2008;4:1637-45.